Structural Engineering and Mechanics, *Vol. 86, No. 1 (2023) 69-83*
https://doi.org/10.12989/sem.2023.86.1.069

Analytical solutions for vibrations of rectangular functionally graded Mindlin plates with vertical cracks

Chiung-Shiann Huang* and Yun-En Lu[a]

Department of Civil Engineering, National Yang Ming Chiao Tung University, Hsinchu, Taiwan

(*Received December 14, 2022, Revised March 6, 2023, Accepted March 7, 2023*)

Abstract. Analytical solutions to problems are crucial because they provide high-quality comparison data for assessing the accuracy of numerical solutions. Benchmark analytical solutions for the vibrations of cracked functionally graded material (FGM) plates are not available in the literature because of the high level of complexity of such solutions. On the basis of first-order shear deformation plate theory (FSDT), this study proposes analytical series solutions for the vibrations of FGM rectangular plates with side or internal cracks parallel to an edge of the plates by using Fourier cosine series and the domain decomposition technique. The distributions of FGM properties along the thickness direction are assumed to follow a simple power law. The proposed analytical series solutions are validated by performing comprehensive convergence studies on the vibration frequencies of cracked square plates with various crack lengths and under various boundary condition combinations and by performing comparisons with published results based on various plate theories and the theory of three-dimensional elasticity. The results reveal that the proposed solutions are in excellent agreement with literature results obtained using the Ritz method on the basis of FSDT. The paper also presents tabulations of the first six nondimensional frequencies of cracked rectangular Al/Al2O3 FGM plates with various aspect ratios, thickness-to-width ratios, crack lengths, and FGM power law indices under six boundary condition combinations, the tabulated frequencies can serve as benchmark data for assessing the accuracy of numerical approaches based on FSDT.

Keywords: analytical solution; FGM cracked rectangular plates; first-order shear deformation plate theory; vibration

1. Introduction

Plates are widely used as structural components, but they can crack because of material flaws, ceaselessly irregular loads induced by waves, or cyclic loads from a machine. The presence of a crack can considerably change the dynamic characteristics of a plate. Consequently, investigating the dynamic characteristics of cracked plates is crucial for avoiding resonance, which can cause a plate to malfunction, and for developing vibration-based plate crack identification techniques.

A vast number of studies have applied various plate theories and the theory of three-dimensional elasticity to demonstrate the influence of crack length, location, and orientation on the vibrations of cracked homogeneous plates. On the basis of classic plate theory (CPT), researchers have analyzed the vibrations of cracked rectangular plates by solving Fredholm integral equations for plates with simply supported boundary conditions (Lynn and Kumbasar 1967, Stahl and Keer 1972, Aggarwala and Ariel 1981) and using the Ritz method (Yuan and Dickinson 1992, Liew *et al.* 1994, Huang and Leissa 2009), extended finite element method (XFEM, Bachene *et al.* 2009), generalized differential quadrature element method (Shahverdi and Navardi 2017), and extended isogeometric analysis (XIGA, Yang and Dong 2019) for plates with various combinations of boundary conditions. Similarly, on the basis of first-order shear deformation plate theory (FSDT), the Ritz method (Lee and Lim 1993, Huang *et al.* 2011a), differential quadrature element method (Liu and Liew 1999), FEM (Azam *et al.* 2017), XFEM (Yang *et al.* 2017), mesh-free approach (Peng *et al.* 2017), and phase-field method (Doan *et al.* 2019) have been employed to find the natural frequencies of rectangular plates with various crack configurations and under various combinations of boundary conditions. Notably, Hosseini-Hashemi *et al.* (2010) presented analytical solutions for rectangular plates with two opposite edges simply supported and having all-over part-through open cracks perpendicular to two opposite simply supported edges.

Over the past three decades, functionally graded materials (FGMs) have been applied in diverse fields because they can be designed easily to meet various rigorous engineering requirements such as high resistance to temperature gradients and corrosion, high toughness, and high strength without the disadvantage of stress concentration encountered in conventional laminated composite materials. Consequently, numerous studies have investigated the vibrations of FGM plates with cracks and have proposed various numerical solutions (Swaminathan *et al.* 2015, Zhang *et al.* 2019, Gayen *et al.* 2019, Sinha and Kumar 2020). For example, based on CPT, Joshi *et al.* (2015) studied vibrations of orthotropic FGM rectangular

*Corresponding author, Professor
E-mail: cshuang@nycu.edu.tw
[a]M.S. Student
E-mail: mokusho67@gmail.com

ISSN: 1225-4568 (Print), 1598-6217 (Online)

plates with part-through vertical central cracks by using the line spring model to model a crack. On the basis of FSDT, Natarajan *et al.* (2011a), Nguyen-Thoi *et al.* (2017) applied four-node quadrilateral plate-bending elements and cell-based smoothed three-node elements, respectively, to develop extended finite element solutions, moreover, Fantuzzi *et al.* (2015) proposed a generalized differential quadrature finite element solution. Other researchers have performed an extended isogeometric analysis using nonuniform rational B-spline basis functions to determine the natural frequencies of FGM plates with straight and curved internal cracks (Yin *et al.* 2016, Zhang *et al.* 2021, Khalafia and Fazilati 2021). Natarajan *et al.* (2011b) and Rahimabadi *et al.* (2013) used FEM and XFEM, respectively, to investigate the effects of in-plane thermal loading on the vibrations of rectangular FGM plates with internal cracks. In addition, scholars have applied the Ritz method and an extended isogeometric approach to analyze the vibrations of cracked thick FGM plates on the basis of Reddy's third-order shear deformation plate theory (TSDT, Huang *et al.* 2011b, Tran *et al.* 2015, Yang *et al.* 2020) and the theory of three-dimensional elasticity (Huang *et al.* 2012). Minh *et al.* (2021), Minh and Duc (2021) employed the phase-field method and finite element approach in combination with Shi's third-order shear deformation theory to analyze the vibrations of cracked FGM plates with variable thickness, resting on Pasternak elastic foundations and under thermal environment, respectively. In another study, Duc and Minh (2021) investigated the vibrations of FG carbon nanotubes reinforced composite plates with cracks. On the basis of higher-order shear deformation theory (HSDT), Raza *et al.* (2021) investigated the influence of material uncertainty on the vibration characteristics of cracked FGM plates by using extended stochastic finite element formulation. Huang *et al.* (2021) further adapted the moving least-square (MLS) Ritz method to study the effects of in-plane loading on the three-dimensional vibrations of cracked rectangular plates.

According to our review of the literature, analytical solutions for the vibrations of cracked FGM plates have yet been developed. A crack complicates the development of analytical solutions for the vibration of plates with simple geometries such as rectangular or circular plates. Accordingly, to fill this research gap, the present study applies FSDT to develop analytical series solutions for the vibrations of rectangular FGM plates with cracks parallel to the plate edge. These analytical solutions are established by decomposing a cracked plate into four or six subdomains and expressing the displacement fields in each subdomain in terms of a set of cosine Fourier series and polynomial auxiliary functions. The analytical solutions satisfy the governing equations, boundary conditions, and continuity conditions without an approximation. The solutions are validated by performing comprehensive convergence studies involving plates with side or internal cracks under four combinations of boundary conditions and by comparing the obtained vibration frequencies with those published in the literature. To provide benchmark data for evaluating solutions obtained using various numerical methods, this paper presents tabulations of the nondimensional vibration frequencies of rectangular

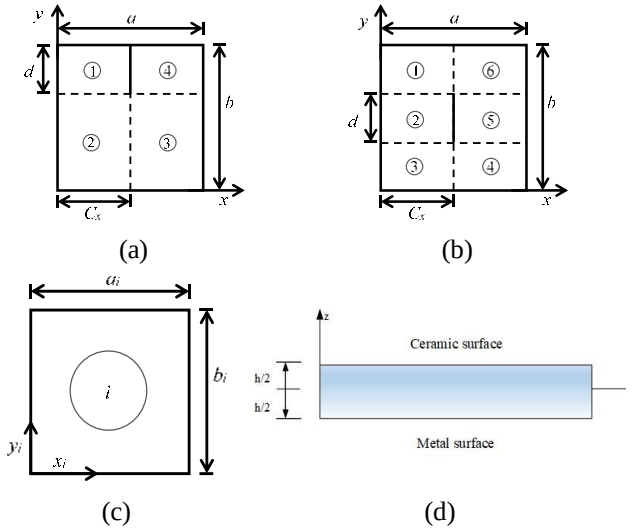

Fig. 1 (a) Top view of a side-cracked plate, (b) Top view of an internally cracked plate, (c) Subdomain *i* with local coordinates, (d) Side view of an FGM plate

Al/Al_2O_3 FGM plates with side and internal cracks of various lengths under various boundary condition combinations. Additionally, the effects of the thickness-to-side ratio, aspect ratio, and material gradient index on the vibration frequencies of cracked plates are investigated.

2. Basic equations

Fig. 1 illustrates a rectangular FGM plate of length a, width b, thickness h, and vertical side or internal crack length d. Herein, a side-cracked plate and an internally cracked plate are decomposed into four and six rectangular subdomains, respectively. Each rectangular subdomain has its own local coordinates. For example, the local coordinates of a rectangular subdomain i of length a_i and width b_i are (x_i, y_i).

Assume that FGM plates exhibit smooth, continuous variation of material properties in the thickness direction. The distribution of material properties follows the simple power law

$$P(z) = (P_c - P_m)V(z) + P_m \text{ and } V(z) = (\frac{z}{h} + \frac{1}{2})^{\bar{m}}, \quad (1)$$

where P_c and P_m denote the properties (elastic modulus E, Poisson's ratio ν, and mass density ρ) of ceramic and metal materials, respectively, and $\bar{m}$ denotes the power-law index governing material property variations along the z direction. The FGM plates under consideration are composed of Al and Al_2O_3, and their material properties are outlined as follows:

Al: E=70 Gpa, ν=0.3, ρ= 2702 kg/m^3,

Al_2O_3: E=380 Gpa, ν=0.3, ρ= 3800 kg/m^3.

On the basis of FSDT, the displacement field in subdomain i can be expressed as follows

$$\bar{u}^{(i)}(x_i, y_i, z, t) = u_0^{(i)}(x_i, y_i, t) + z\psi_x^{(i)}(x_i, y_i, t), \quad (2a)$$

$$\bar{v}^{(i)}(x_i, y_i, z, t) = v_0^{(i)}(x_i, y_i, t) + z\psi_y^{(i)}(x_i, y_i, t), \quad (2b)$$

$$\bar{w}^{(i)}(x_i, y_i, z, t) = w^{(i)}(x_i, y_i, t), \tag{2c}$$

where $\bar{u}^{(i)}$, $\bar{v}^{(i)}$, and $\bar{w}^{(i)}$ are the displacement components along the x_i, y_i, and z directions, respectively, $u_0^{(i)}$, $v_0^{(i)}$, and $w^{(i)}$ are the displacements in the midplane, and $\psi_x^{(i)}$ and $\psi_y^{(i)}$ are rotations of the midplane normal along the x_i and y_i directions, respectively. The stress resultants in subdomain *i* can be defined as follows

$$Q_\beta^{(i)} = \int_{-h/2}^{h/2} \sigma_{\beta z}^{(i)}\, dz, \begin{Bmatrix} N_{\beta\beta}^{(i)} \\ M_{\beta\beta}^{(i)} \end{Bmatrix} = \int_{-h/2}^{h/2} \sigma_{\beta\beta}^{(i)} \begin{Bmatrix} 1 \\ z \end{Bmatrix} dz,$$
$$\begin{Bmatrix} N_{xy}^{(i)} \\ M_{xy}^{(i)} \end{Bmatrix} = \int_{-h/2}^{h/2} \sigma_{xy}^{(i)} \begin{Bmatrix} 1 \\ z \end{Bmatrix} dz, \tag{3}$$

where the subscript β represents x or y and σ_{ij} represents the stress components. The equations of motion can be expressed as follows (Mindlin 1951)

$$N_{xx,x_i}^{(i)} + N_{xy,y_i}^{(i)} = I_0 \ddot{u}_0^{(i)} + I_1 \ddot{\psi}_x^{(i)}, \tag{4a}$$

$$N_{xy,x_i}^{(i)} + N_{yy,y_i}^{(i)} = I_0 \ddot{v}_0^{(i)} + I_1 \ddot{\psi}_y^{(i)}, \tag{4b}$$

$$Q_{x,x_i}^{(i)} + Q_{y,y_i}^{(i)} = I_0 \ddot{w}^{(i)}, \tag{4c}$$

$$M_{xx,x_i}^{(i)} + M_{xy,y_i}^{(i)} - Q_x^{(i)} = I_1 \ddot{u}_0^{(i)} + I_2 \ddot{\psi}_x^{(i)}, \tag{4d}$$

$$M_{xy,x_i}^{(i)} + M_{yy,y_i}^{(i)} - Q_y^{(i)} = I_1 \ddot{v}_0^{(i)} + I_2 \ddot{\psi}_y^{(i)}, \tag{4e}$$

where $I_j = \int_{-h/2}^{h/2} \rho(z) z^j\, dz$, and the subscript comma denotes partial differentiation with respect to the coordinate defined by the variable after the comma.

Substituting the linear strain-displacement relationship (Eq. (5))

$$\begin{Bmatrix} \varepsilon_{xx}^{(i)} \\ \varepsilon_{yy}^{(i)} \\ 2\varepsilon_{xy}^{(i)} \\ 2\varepsilon_{xz}^{(i)} \\ 2\varepsilon_{yz}^{(i)} \end{Bmatrix} = \begin{Bmatrix} u_{0,x_i}^{(i)} \\ v_{0,y_i}^{(i)} \\ u_{0,y_i}^{(i)} + v_{0,x_i}^{(i)} \\ \psi_x^{(i)} + w_{,x_i}^{(i)} \\ \psi_y^{(i)} + w_{,y_i}^{(i)} \end{Bmatrix} + z \begin{Bmatrix} \psi_{x,x_i}^{(i)} \\ \psi_{y,y_i}^{(i)} \\ \psi_{x,y_i}^{(i)} + \psi_{y,x_i}^{(i)} \\ 0 \\ 0 \end{Bmatrix} \tag{5}$$

and the stress-strain relationship (Eq. (6))

$$\begin{Bmatrix} \sigma_{xx}^{(i)} \\ \sigma_{yy}^{(i)} \\ \sigma_{xy}^{(i)} \\ \sigma_{xz}^{(i)} \\ \sigma_{yz}^{(i)} \end{Bmatrix} = \begin{bmatrix} \frac{E}{1-\nu^2} & \frac{\nu E}{1-\nu^2} & 0 & 0 & 0 \\ \frac{\nu E}{1-\nu^2} & \frac{E}{1-\nu^2} & 0 & 0 & 0 \\ 0 & 0 & 2G & 0 & 0 \\ 0 & 0 & 0 & 2G & 0 \\ 0 & 0 & 0 & 0 & 2G \end{bmatrix} \begin{Bmatrix} \varepsilon_{xx}^{(i)} \\ \varepsilon_{yy}^{(i)} \\ \varepsilon_{xy}^{(i)} \\ \varepsilon_{xz}^{(i)} \\ \varepsilon_{yz}^{(i)} \end{Bmatrix} \tag{6}$$

into Eq. (3) yields the following expressions

$$N_{xx}^{(i)} = \bar{E}_0 u_{0,x_i}^{(i)} + \bar{E}_1 \psi_{x,x_i}^{(i)} + \bar{D}_0 v_{0,y_i}^{(i)} + \bar{D}_1 \psi_{y,y_i}^{(i)}, \tag{7a}$$

$$N_{yy}^{(i)} = \bar{D}_0 u_{0,x_i}^{(i)} + \bar{D}_1 \psi_{x,x_i}^{(i)} + \bar{E}_0 v_{0,y_i}^{(i)} + \bar{E}_1 \psi_{y,y_i}^{(i)}, \tag{7b}$$

$$N_{xy}^{(i)} = \bar{G}_0 (u_{0,y_i}^{(i)} + v_{0,x_i}^{(i)}) + \bar{G}_1 (\psi_{x,y_i}^{(i)} + \psi_{y,x_i}^{(i)}), \tag{7c}$$

$$M_{xx}^{(i)} = \bar{E}_1 u_{0,x_i}^{(i)} + \bar{E}_2 \psi_{x,x_i}^{(i)} + \bar{D}_1 v_{0,y_i}^{(i)} + \bar{D}_2 \psi_{y,y_i}^{(i)}, \tag{7d}$$

$$M_{yy}^{(i)} = \bar{D}_1 u_{0,x_i}^{(i)} + \bar{D}_2 \psi_{x,x_i}^{(i)} + \bar{E}_1 v_{0,y_i}^{(i)} + \bar{E}_2 \psi_{y,y_i}^{(i)}, \tag{7e}$$

$$M_{xy}^{(i)} = \bar{G}_1 (u_{0,y_i}^{(i)} + v_{0,x_i}^{(i)}) + \bar{G}_2 (\psi_{x,y_i}^{(i)} + \psi_{y,x_i}^{(i)}), \tag{7f}$$

$$Q_x^{(i)} = \kappa \bar{G}_0 (w_{,x_i}^{(i)} + \psi_x^{(i)}), \tag{7g}$$

$$Q_y^{(i)} = \kappa \bar{G}_0 (w_{,y_i}^{(i)} + \psi_y^{(i)}), \tag{7h}$$

where

$$\bar{G}_j = \int_{-h/2}^{h/2} G z^j\, dz,\ \bar{E}_j = \int_{-h/2}^{h/2} \frac{E}{1-\nu^2} z^j\, dz,$$
$$\bar{D}_j = \int_{-h/2}^{h/2} \frac{\nu E}{1-\nu^2} z^j\, dz. \tag{8}$$

The transverse shear correction coefficient κ is assumed to be $5/6$ without special mention.

Substituting Eq. (7) into Eq. (4) yields the following governing equations in terms of displacement functions

$$\bar{E}_0 u_{0,x_i x_i}^{(i)} + \bar{E}_1 \psi_{x,x_i x_i}^{(i)} + \bar{D}_0 v_{0,x_i y_i}^{(i)} + \bar{D}_1 \psi_{y,x_i y_i}^{(i)} + \bar{G}_0 (u_{0,y_i y_i}^{(i)} + v_{0,x_i y_i}^{(i)}) + \bar{G}_1 (\psi_{x,y_i y_i}^{(i)} + \psi_{y,x_i y_i}^{(i)}) = I_0 \ddot{u}_0^{(i)} + I_1 \ddot{\psi}_x^{(i)}, \tag{9a}$$

$$\bar{D}_0 u_{0,x_i y_i}^{(i)} + \bar{D}_1 \psi_{x,x_i y_i}^{(i)} + \bar{E}_0 v_{0,y_i y_i}^{(i)} + \bar{E}_1 \psi_{y,y_i y_i}^{(i)} + \bar{G}_0 (u_{0,x_i y_i}^{(i)} + v_{0,x_i x_i}^{(i)}) + \bar{G}_1 (\psi_{x,x_i y_i}^{(i)} + \psi_{y,x_i x_i}^{(i)}) = I_0 \ddot{v}_0^{(i)} + I_1 \ddot{\psi}_y^{(i)}, \tag{9b}$$

$$\kappa \bar{G}_0 \left[(w_{0,x_i x_i}^{(i)} + \psi_{x,x_i}^{(i)}) + (w_{0,y_i y_i}^{(i)} + \psi_{y,y_i}^{(i)}) \right] = I_0 \ddot{w}_0^{(i)}, \tag{9c}$$

$$\bar{E}_1 u_{0,x_i x_i}^{(i)} + \bar{E}_2 \psi_{x,x_i x_i}^{(i)} + \bar{D}_1 v_{0,x_i y_i}^{(i)} + \bar{D}_2 \psi_{y,x_i y_i}^{(i)} + \bar{G}_1 (u_{0,y_i y_i}^{(i)} + v_{0,x_i y_i}^{(i)}) + \bar{G}_2 (\psi_{x,y_i y_i}^{(i)} + \psi_{y,x_i y_i}^{(i)}) - \kappa \bar{G}_0 (w_{0,x_i}^{(i)} + \psi_x^{(i)}) = I_1 \ddot{u}_0^{(i)} + I_2 \ddot{\psi}_x^{(i)}, \tag{9d}$$

$$\bar{D}_1 u_{0,x_i y_i}^{(i)} + \bar{D}_2 \psi_{x,x_i y_i}^{(i)} + \bar{E}_1 v_{0,y_i y_i}^{(i)} + \bar{E}_2 \psi_{y,y_i y_i}^{(0)} + \bar{G}_1 (u_{0,x_i y_i}^{(i)} + v_{0,x_i x_i}^{(i)}) + \bar{G}_2 (\psi_{x,x_i y_i}^{(i)} + \psi_{y,x_i x_i}^{(i)}) - \kappa \bar{G}_0 (w_{0,y_i}^{(i)} + \psi_y^{(i)}) = I_1 \ddot{v}_0^{(i)} + I_2 \ddot{\psi}_y^{(i)}, \tag{9e}$$

3. Series solutions

The Fourier cosine series are adapted herein to establish analytical series solutions for the vibrations of cracked FGM rectangular plates. In subdomain *i* of the cracked plate displayed in Fig. 1, let

$$u_0^{(i)}(x_i, y_i, t) = U_0^{(i)}(x_i, y_i) \cdot e^{i\omega t},$$
$$v_0^{(i)}(x_i, y_i, t) = V_0^{(i)}(x_i, y_i) \cdot e^{i\omega t},$$
$$w_0^{(i)}(x_i, y_i, t) = W_0^{(i)}(x_i, y_i) \cdot e^{i\omega t},$$
$$\psi_x^{(i)}(x_i, y_i, t) = \Psi_x^{(i)}(x_i, y_i) \cdot e^{i\omega t},$$
$$\psi_y^{(i)}(x_i, y_i, t) = \Psi_y^{(i)}(x_i, y_i) \cdot e^{i\omega t}, \tag{10}$$

and

$$U_0^{(i)}(x_i, y_i) = \sum_{m=0}^{M_i} \sum_{n=0}^{N_i} A_{mn}^{(i,1)} \cos \alpha_m^{(i)} x_i \cos \beta_n^{(i)} y_i + \sum_{l=1}^{2} \xi_l^{(i)}(x_i) \sum_{n=0}^{N_i} B_{ln}^{(i,1)} \cos \beta_n^{(i)} y_i + \sum_{l=1}^{2} \eta_l^{(i)}(y_i) \sum_{m=0}^{M_i} C_{lm}^{(i,1)} \cos \alpha_m^{(i)} x_i \tag{11a}$$

$$V_0^{(i)}(x_i,y_i)=\sum_{m=0}^{M_i}\sum_{n=0}^{N_i}A_{mn}^{(i,2)}\cos\alpha_m^{(i)}x_i\cos\beta_n^{(i)}y_i+\sum_{l=1}^{2}\xi_l^{(i)}(x_i)\sum_{n=0}^{N_i}B_{ln}^{(i,2)}\cos\beta_n^{(i)}y_i+\sum_{l=1}^{2}\eta_l^{(i)}(y_i)\sum_{m=0}^{M_i}C_{lm}^{(i,2)}\cos\alpha_m^{(i)}x_i \tag{11b}$$

$$W_0^{(i)}(x_i,y_i)=\sum_{m=0}^{M_i}\sum_{n=0}^{N_i}A_{mn}^{(i,3)}\cos\alpha_m^{(i)}x_i\cos\beta_n^{(i)}y_i+\sum_{l=1}^{2}\xi_l^{(i)}(x_i)\sum_{n=0}^{N_i}B_{ln}^{(i,3)}\cos\beta_n^{(i)}y_i+\sum_{l=1}^{2}\eta_l^{(i)}(y_i)\sum_{m=0}^{M_i}C_{lm}^{(i,3)}\cos\alpha_m^{(i)}x_i \tag{11c}$$

$$\Psi_x^{(i)}(x_i,y_i)=\sum_{m=0}^{M_i}\sum_{n=0}^{N_i}A_{mn}^{(i,4)}\cos\alpha_m^{(i)}x_i\cos\beta_n^{(i)}y_i+\sum_{l=1}^{2}\xi_l^{(i)}(x_i)\sum_{n=0}^{N_i}B_{ln}^{(i,4)}\cos\beta_n^{(i)}y_i+\sum_{l=1}^{2}\eta_l^{(i)}(y_i)\sum_{m=0}^{M_i}C_{lm}^{(i,4)}\cos\alpha_m^{(i)}x_i \tag{11d}$$

$$\Psi_y^{(i)}(x_i,y_i)=\sum_{m=0}^{M_i}\sum_{n=0}^{N_i}A_{mn}^{(i,5)}\cos\alpha_m^{(i)}x_i\cos\beta_n^{(i)}y_i+\sum_{l=1}^{2}\xi_l^{(i)}(x_i)\sum_{n=0}^{N_i}B_{ln}^{(i,5)}\cos\beta_n^{(i)}y_i+\sum_{l=1}^{2}\eta_l^{(i)}(y_i)\sum_{m=0}^{M_i}C_{lm}^{(i,5)}\cos\alpha_m^{(i)}x_i, \tag{11e}$$

where $\alpha_m^{(i)}=m\pi/a_i$, $\beta_n^{(i)}=n\pi/b_i$, $A_{mn}^{(i,j)}, B_{ln}^{(i,j)}$ and $C_{lm}^{(i,j)}$ are the coefficients to be determined. Moreover, $\xi_l^{(i)}(x_i)$ and $\eta_l^{(i)}(y_i)$ are supplementary polynomial functions, which satisfy the following conditions (Li 2000, Li *et al.* 2009)

$$\xi_{1,x_i}^{(i)}(0)=1,\ \xi_{1,x_i}^{(i)}(a_i)=0,\ \xi_{2,x_i}^{(i)}(0)=0,\ \xi_{2,x_i}^{(i)}(a_i)=1,\ \eta_{1,y_i}^{(i)}(0)=1,\ \eta_{1,y_i}^{(i)}(b_i)=0,\ \eta_{2,y_i}^{(i)}(0)=0,\eta_{2,y_i}^{(i)}(b_i)=1,\ \int_0^{a_i}\xi_l^{(i)}(x_i)dx_i=0 \text{ and } \int_0^{b_i}\eta_l^{(i)}(y_i)dy_i=0\ (l=1,2). \tag{12}$$

Consequently

$$\xi_1^{(i)}(x_i)=-\frac{{x_i}^2}{2a_i}+x_i-\frac{a_i}{3},\ \xi_2^{(i)}(x_i)=\frac{{x_i}^2}{2a_i}-\frac{a_i}{6},\quad \eta_1^{(i)}(y_i)=-\frac{{y_i}^2}{2b_i}+y_i-\frac{b_i}{3},\ \eta_2^{(i)}(y_i)=\frac{{y_i}^2}{2b_i}-\frac{b_i}{6}. \tag{13}$$

Establishing the desired analytical solutions involves two main steps. The first step entails satisfying the boundary conditions and continuity conditions between two adjacent subdomains and determining the relationships between the sets of coefficients $\{A_{mn}^{(i,j)}|j=1\sim5, i=1\sim4\ (\text{or } 6),\ m=0\sim M_i,\ n=0\sim N_i\}$ and $\{B_{ln}^{(i,j)},\ C_{lm}^{(i,j)}|j=1\sim5, i=1\sim4\ (\text{or } 6),\ l=1 \text{ and } 2,\ m=0\sim M_i,\ n=0\sim N_i\}$. Notably, the continuity conditions consist of the continuities of the displacement and rotation components and the stress resultants. For instance, satisfying the boundary condition $v_0^{(i)}(x_i,y_i,t)=0$ at $x_i=a_i$ yields $V_0^{(i)}(a_i,y_i)=0$, which gives

$$\sum_{n=0}^{N_i}[\sum_{m=0}^{M_i}A_{mn}^{(i,2)}\cos\alpha_m^{(i)}a_i+\sum_{l=1}^{2}\xi_l^{(i)}(a_i)B_{ln}^{(i,2)}+\sum_{l=1}^{2}\bar{c}_{ln}^{(i)}\sum_{m=0}^{M_i}C_{lm}^{(i,2)}\cos\alpha_m^{(i)}a_i]\cos\beta_n^{(i)}y_i=0 \tag{14}$$

Here, $\bar{c}_{ln}^{(i)}$ is determined from ${\eta_l}^{(i)}(y_i)$, where ${\eta_l}^{(i)}(y_i)=\sum_{n=0}^{N_i}\bar{c}_{ln}^{(i)}\cos\beta_n^{(i)}y_i$ and $\bar{c}_{ln}^{(i)}=\frac{\int_0^{b_i}\eta_l^{(i)}(y_i)\cos\beta_n^{(i)}y_i dy_i}{\int_0^{b_i}(\cos\beta_n^{(i)}y_i)^2dy_i}$. Eq. (14) must be satisfied for all y_i in $[0, b_i]$, and this results in

$$\sum_{m=0}^{M_i}A_{mn}^{(i,2)}\cos\alpha_m^{(i)}a_i+\sum_{l=1}^{2}\xi_l^{(i)}(a_i)B_{ln}^{(i,2)}+\sum_{l=1}^{2}\bar{c}_{ln}^{(i)}\sum_{m=0}^{M_i}C_{lm}^{(i,2)}\cos\alpha_m^{(i)}a_i=0 \quad (n=0, 1, \ldots, N_i). \tag{15}$$

Ten continuity conditions exist along a common edge of two adjacent subdomains. Consider the continuity of M_{yy} along a common horizontal edge of two adjacent subdomains i and j, where $y_i=b_i$ and $y_j=0$ along the edge. Substituting Eqs. (7e), (11), and (13) into $M_{yy}^{(i)}(x_i,b_i,t)=M_{yy}^{(j)}(x_j,0,t)$ yields

$$\begin{aligned}&\sum_{n=0}^{N_i}\sum_{m=0}^{M_i}\alpha_m^{(i)}(-\bar{D}_1A_{mn}^{(i,1)}-\bar{D}_2A_{mn}^{(i,4)})\sin\alpha_m^{(i)}x_i\cos\beta_n^{(i)}b_i+\sum_{l=1}^{2}\eta_l^{(i)}(b_i)\sum_{m=0}^{M_i}\alpha_m^{(i)}\big(-\bar{D}_1C_{lm}^{(i,1)}-\bar{D}_2C_{lm}^{(i,4)}\big)\sin\alpha_m^{(i)}x_{i+}\sum_{l=1}^{2}\xi_{l,x_i}^{(i)}(x_i)\sum_{n=0}^{N_i}\big(\bar{D}_1B_{ln}^{(i,1)}+\bar{D}_2B_{ln}^{(i,4)}\big)\cos\beta_n^{(i)}b_i+\sum_{m=0}^{M_i}\sum_{n=0}^{N_i}\beta_n^{(i)}\big(-\bar{E}_1A_{mn}^{(i,2)}-\bar{E}_2A_{mn}^{(i,5)}\big)\sin\beta_n^{(i)}b_i\cos\alpha_m^{(i)}x_i+\sum_{l=1}^{2}\xi_l^{(i)}(x_i)\sum_{n=0}^{N_i}\beta_n^{(i)}\big(-\bar{E}_1B_{ln}^{(i,2)}-\bar{E}_2B_{ln}^{(i,5)}\big)\sin\beta_n^{(i)}b_i+\sum_{l=1}^{2}\eta_{l,y_i}^{(i)}(b_i)\sum_{m=0}^{M_i}(\bar{E}_1C_{lm}^{(i,2)}+\bar{E}_2C_{lm}^{(i,5)})\cos\alpha_m^{(i)}x_i=\sum_{n=0}^{N_j}\sum_{m=0}^{M_j}\alpha_m^{(j)}\big(-\bar{D}_1A_{mn}^{(j,1)}-\bar{D}_2A_{mn}^{(j,4)}\big)\sin\alpha_m^{(j)}x_j+\sum_{l=1}^{2}\xi_{l,x_j}^{(j)}(x_j)\sum_{n=0}^{N_j}(\bar{D}_1B_{ln}^{(j,1)}+\bar{D}_2B_{ln}^{(j,4)})+\sum_{l=1}^{2}\eta_l^{(j)}(0)\sum_{m=0}^{M_j}\alpha_m^{(j)}(-\bar{D}_1C_{lm}^{(j,1)}-\bar{D}_2C_{lm}^{(j,4)})\sin\alpha_m^{(j)}x_j]+\sum_{l=1}^{2}\eta_{l,y_j}^{(j)}(0)\sum_{m=0}^{M_j}(\bar{E}_1C_{lm}^{(j,2)}+\bar{E}_2C_{lm}^{(j,5)})\cos\alpha_m^{(j)}x_j.\end{aligned} \tag{16}$$

For simplicity, let $M_i=M_j$. The functions of x_i and x_j in Eq. (16) can be expanded in terms of Fourier cosine series as follows

$$\xi_l^{(k)}(x_k)=\sum_{m=0}^{M_k}\bar{b}_{lm}^{(k)}\cos\alpha_m^{(k)}x_k,\quad \xi_{l,x_k}^{(k)}(x_k)=\sum_{m=0}^{M_k}\hat{b}_{lm}^{(k)}\cos\alpha_m^{(k)}x_k,\quad \sin\alpha_p^{(k)}x_k=\sum_{m=0}^{M_k}\bar{S}_{xmp}^{(k)}\cos\alpha_m^{(k)}x_k\ (k=i \text{ or } j) \tag{17}$$

Introducing Eq. (17) into Eq. (16) yields

$$\begin{aligned}&\sum_{n=0}^{N_i}\sum_{p=0}^{M_i}\alpha_p^{(i)}(-\bar{D}_1A_{pn}^{(i,1)}-\bar{D}_2A_{pn}^{(i,4)})\bar{S}_{xmp}^{(i)}\cos\beta_n^{(i)}b_i+\sum_{l=1}^{2}\hat{b}_{lm}^{(i)}\sum_{n=0}^{N_i}(\bar{D}_1B_{ln}^{(i,1)}+\bar{D}_2B_{ln}^{(i,4)})\cos\beta_n^{(i)}b_i+\sum_{l=1}^{2}\eta_l^{(i)}(b_i)\sum_{p=0}^{M_i}\alpha_p^{(i)}\big(-\bar{D}_1C_{lp}^{(i,1)}-\bar{D}_2C_{lp}^{(i,4)}\big)\bar{S}_{xmp}^{(i)}+\sum_{n=0}^{N_i}\beta_n^{(i)}(-\bar{E}_1A_{mn}^{(i,2)}-\bar{E}_2A_{mn}^{(i,5)})\sin\beta_n^{(i)}b_i+\sum_{l=1}^{2}\bar{b}_{lm}^{(i)}\sum_{n=0}^{N_i}\beta_n^{(i)}\big(-\bar{E}_1B_{ln}^{(i,2)}-\bar{E}_2B_{ln}^{(i,5)}\big)\sin\beta_n^{(i)}b_i+\sum_{l=1}^{2}\eta_{l,y_i}^{(i)}(b_i)(\bar{E}_1C_{lm}^{(i,2)}+\bar{E}_2C_{lm}^{(i,5)})=\sum_{n=0}^{N_i}\sum_{p=0}^{M_i}\alpha_p^{(j)}\big(-\bar{D}_1A_{pn}^{(j,1)}-\bar{D}_2A_{pn}^{(j,4)}\big)\bar{S}_{xmp}^{(j)}+\sum_{l=1}^{2}\hat{b}_{lm}^{(j)}\sum_{n=0}^{N_j}(\bar{D}_1B_{ln}^{(j,1)}+\bar{D}_2B_{ln}^{(j,4)})\cos\beta_n^{(j)}b_i+\sum_{l=1}^{2}\eta_l^{(j)}(0)\sum_{p=0}^{M_i}\alpha_p^{(j)}\big(-\bar{D}_1C_{lp}^{(j,1)}-\bar{D}_2C_{lp}^{(j,4)}\big)\bar{S}_{xmp}^{(j)}+\sum_{l=1}^{2}\eta_{l,y_j}^{(j)}(0)(\bar{E}_1C_{lm}^{(j,2)}+\bar{E}_2C_{lm}^{(j,5)})\quad (m=0\sim M_i).\end{aligned} \tag{18}$$

Satisfying the boundary conditions along a horizontal edge and a vertical edge of subdomain *i* yields 5 (M_i+1) and 5 (N_i+1) linear algebraic homogeneous equations for the set of coefficients $\{A_{mn}^{(i,j)}, B_{ln}^{(i,j)}, C_{lm}^{(i,,j)} \mid j = 1\sim5,\ l$=1 and 2, $m = 0\sim M_i, n = 0\sim N_i\}$, respectively. For simplicity, when subdomains *i* and *j* share a common horizontal edge or a common vertical edge, let $M_i = M_j$ or $N_i = N_j$, respectively. Satisfying the continuity conditions along a shared horizontal edge and a shared vertical edge of subdomains *i* and *j* yields 10 (M_i+1) and 10 (N_i+1) linear algebraic homogeneous equations for the coefficients, respectively.

To satisfy the boundary conditions along the crack and the four edges of a rectangular plate and the continuity conditions along the shared edges between every two adjacent subdomains, a total of $\sum_{i=1}^{4} 10(M_i + N_i + 2)$ and $\sum_{i=1}^{6} 10(M_i + N_i + 2)$ linear algebraic homogeneous equations are established for the coefficients of a side-cracked plate and an internally cracked plate, respectively. Consequently, these algebraic equations can be expressed in matrix form as follows

$$\mathbf{B}_{\mathrm{P}}\mathbf{P} = \mathbf{B}_{\mathrm{F}}\mathbf{F}, \tag{19}$$

where

$$\mathbf{P} = (\mathbf{P}^{(1)}\ \mathbf{P}^{(2)}\ \mathbf{P}^{(3)} \cdots\ \mathbf{P}^{(k)})^T, \mathbf{F} = (\mathbf{F}^{(1)}\ \mathbf{F}^{(2)}\ \mathbf{F}^{(3)} \cdots \mathbf{F}^{(k)})^T, \mathbf{F}^{(\mathrm{i})} = (\widetilde{\mathbf{A}}^{(i,1)}\ \widetilde{\mathbf{A}}^{(i,2)} \cdots\ \widetilde{\mathbf{A}}^{(i,5)}),$$
$$\mathbf{P}^{(i)} = (\widetilde{\mathbf{B}}^{(i,1)}\ \widetilde{\mathbf{C}}^{(i,1)}\ \widetilde{\mathbf{B}}^{(i,2)}\ \widetilde{\mathbf{C}}^{(i,2)} \cdots\ \widetilde{\mathbf{B}}^{(i,5)}\ \widetilde{\mathbf{C}}^{(i,5)}),$$
$$\widetilde{\mathbf{B}}^{(i,j)} = (B_{10}^{(i,j)}, B_{11}^{(i,j)}, \cdots, B_{1N_i}^{(i,j)}, B_{20}^{(i,j)}, B_{21}^{(i,j)}, \cdots, B_{2N_i}^{(i,j)}),$$
$$\widetilde{\mathbf{C}}^{(i,j)} = (C_{10}^{(i,j)}, C_{11}^{(i,j)}, \cdots, C_{1M_i}^{(i,j)}, C_{20}^{(i,j)}, C_{21}^{(i,j)}, \cdots, C_{2M_i}^{(i,j)}),$$
$$\widetilde{\mathbf{A}}^{(i,j)} = (A_{00}^{(i,j)}, A_{01}^{(i,j)}, \cdots, A_{0N_i}^{(i,j)}, A_{10}^{(i,j)}, A_{11}^{(i,j)}, \cdots, A_{1N_i}^{(i,j)}, \cdots, A_{M_i0}^{(i,j)}, A_{M_i1}^{(i,j)}, \cdots, A_{M_iN_i}^{(i,j)}),$$

where *k*=4 and 6 for a side-cracked plate and an internally cracked plate, respectively. Applying Eq. (19) yields

$$\mathbf{P} = (\mathbf{B}_{\mathrm{P}}{}^{-1}\mathbf{B}_{\mathrm{F}})\mathbf{F}. \tag{20}$$

The second step in constructing the analytical solutions entails satisfying the governing equations in each subdomain. For example, to satisfy Eq. (9e), Eqs. (11) and (13) should be substituted into Eq. (9e) with careful arrangement to obtain

$$\begin{aligned}
&\sum_{m=0}^{M_i}\sum_{n=0}^{N_i}\{\alpha_m^{(i)}\beta_n^{(i)}[(\bar{D}_1+\bar{G}_1)A_{mn}^{(i,1)} + (\bar{D}_2+\bar{G}_2)A_{mn}^{(i,4)}]\sin\alpha_m^{(i)}x_i\sin\beta_n^{(i)}y_i - [((\beta_n^{(i)})^2\bar{E}_1 + (\alpha_m^{(i)})^2\bar{G}_1)A_{mn}^{(i,2)} + ((\beta_n^{(i)})^2\bar{E}_2 + (\alpha_m^{(i)})^2\bar{G}_2 + \kappa\bar{G}_0)A_{mn}^{(i,5)}]\cos\alpha_m^{(i)}x_i\cos\beta_n^{(i)}y_i + \beta_n^{(i)}\kappa\bar{G}_0A_{mn}^{(i,3)}\cos\alpha_m^{(i)}x_i\sin\beta_n^{(i)}y_i\} + \\
&\sum_{n=0}^{N_i}\sum_{l=1}^{2}\{\beta_n^{(i)}\{-\xi_{l,x_i}^{(i)}(x_i)[(\bar{D}_1+\bar{G}_1)B_{ln}^{(i,1)} + (\bar{D}_2+\bar{G}_2)B_{ln}^{(i,4)}] + \kappa\bar{G}_0\xi_l^{(i)}(x_i)B_{ln}^{(i,3)}\}\sin\beta_n^{(i)}y_i + \{[-(\beta_n^{(i)})^2\bar{E}_1\xi_l^{(i)}(x_i) + \bar{G}_1\xi_{l,x_ix_i}^{(i)}(x_i)]B_{ln}^{(i,2)} + [-((\beta_n^{(i)})^2\bar{E}_2 + \kappa\bar{G}_0)\xi_l^{(i)}(x_i) + \bar{G}_2\xi_{l,x_ix_i}^{(i)}(x_i)]B_{ln}^{(i,5)}\}\cos\beta_n^{(i)}y_i\} + \\
&\sum_{m=0}^{M_i}\sum_{l=1}^{2}\{-\alpha_m^{(i)}\eta_{l,y_i}^{(i)}(y_i)[(\bar{D}_1+\bar{G}_1)C_{lm}^{(i,1)} + (\bar{D}_2+\bar{G}_2)C_{lm}^{(i,4)}]\sin\alpha_m^{(i)}x_i + \{[\bar{E}_1\eta_{l,y_iy_i}^{(i)}(y_i) - (\alpha_m^{(i)})^2\bar{G}_1\eta_l^{(i)}(y_i)]C_{lm}^{(i,2)} - \kappa\bar{G}_0\eta_{l,y_i}^{(i)}(y_i)C_{lm}^{(i,3)}\}\cos\alpha_m^{(i)}x_i + [\bar{E}_2\eta_{l,y_iy_i}^{(i)}(y_i) - ((\alpha_m^{(i)})^2\bar{G}_2 + \kappa\bar{G}_0)\eta_l^{(i)}(y_i)]C_{lm}^{(i,5)}\cos\alpha_m^{(i)}x_i\} = \\
&-\omega^2\{\sum_{m=0}^{M_i}\sum_{n=0}^{N_i}(I_1A_{mn}^{(i,2)} + I_2A_{mn}^{(i,5)})\cos\alpha_m^{(i)}x_i\cos\beta_n^{(i)}y_i + \sum_{l=1}^{2}\xi_l^{(i)}(x_i)\sum_{n=0}^{N_i}(I_1B_{ln}^{(i,2)} + I_2B_{ln}^{(i,5)})\cos\beta_n^{(i)}y_i + \sum_{l=1}^{2}\eta_l^{(i)}(y_i)\sum_{m=0}^{M_i}(I_1C_{lm}^{(i,2)} + I_2C_{lm}^{(i,5)})\cos\alpha_m^{(i)}x_i\}.
\end{aligned} \tag{21}$$

The functions of x_i and y_i are expanded using the Fourier cosine series as follows

$$\begin{aligned}
&\xi_{l,x_ix_i}^{(i)}(x_i) = \sum_{m=0}^{M_i}\tilde{b}_{lm}^{(i)}\cos\alpha_m^{(i)}x_i,\ \eta_l^{(i)}(y_i) = \sum_{n=0}^{N_i}\bar{c}_{ln}^{(i)}\cos\beta_n^{(i)}y_i,\ \eta_{l,y_i}^{(i)}(y_i) = \sum_{n=0}^{N_i}\hat{c}_{ln}^{(i)}\cos\beta_n^{(i)}y_i,\\
&\eta_{l,y_iy_i}^{(i)}(y_i) = \sum_{n=0}^{N_i}\tilde{c}_{ln}^{(i)}\cos\beta_n^{(i)}y_i,\\
&\sin\alpha_p^{(i)}x_i\sin\beta_q^{(i)}y_i = \sum_{m=0}^{M_i}\sum_{n=0}^{N_i}\bar{s}_{mnpq}^{(i)}\cos\alpha_m^{(i)}x_i\cos\beta_n^{(i)}y_i,\\
&\sin\beta_q^{(i)}y_i = \sum_{n=0}^{N_i}\bar{S}_{ynq}^{(i)}\cos\beta_n^{(i)}y_i.
\end{aligned} \tag{22}$$

Substituting Eqs. (17) and (22) into Eq. (21) with careful arrangement yields

$$\begin{aligned}
&-[(\beta_n^{(i)})^2\bar{E}_1 + (\alpha_m^{(i)})^2\bar{G}_1]A_{mn}^{(i,2)} - [(\beta_n^{(i)})^2\bar{E}_2 + (\alpha_m^{(i)})^2\bar{G}_2 + \kappa\bar{G}_0]A_{mn}^{(i,5)} + \sum_{q=0}^{N_i}\beta_q^{(i)}\kappa\bar{G}_0\bar{S}_{ynq}^{(i)}A_{mq}^{(i,3)} + \sum_{p=0}^{M_i}\sum_{q=0}^{N_i}\alpha_p^{(i)}\beta_q^{(i)}\bar{s}_{mnpq}^{(i)}[(\bar{D}_1+\bar{G}_1)A_{pq}^{(i,1)} + (\bar{D}_2+\bar{G}_2)A_{pq}^{(i,4)}] + \sum_{l=1}^{2}[-(\beta_n^{(i)})^2\bar{E}_1\,\tilde{b}_{lm}^{(i)} + \bar{G}_1\tilde{b}_{lm}^{(i)}]B_{ln}^{(i,2)} + \{-[(\beta_n^{(i)})^2\bar{E}_2 + \kappa\bar{G}_0]\tilde{b}_{lm}^{(i)} + \bar{G}_2\tilde{b}_{lm}^{(i)}\}B_{ln}^{(i,5)} + \\
&\sum_{q=0}^{N_i}\sum_{l=1}^{2}\beta_q^{(i)}\bar{S}_{ynq}^{(i)}\{-\hat{b}_{lm}^{(i)}[(\bar{D}_1+\bar{G}_1)B_{lq}^{(i,1)} + (\bar{D}_2+\bar{G}_2)B_{lq}^{(i,4)}] + \kappa\bar{G}_0\bar{b}_{lm}^{(i)}B_{lq}^{(i,3)}\} + \sum_{l=1}^{2}[\bar{E}_1\,\tilde{c}_{ln}^{(i)} - (\alpha_m^{(i)})^2\bar{G}_1\tilde{c}_{ln}^{(i)}]C_{lm}^{(i,2)} - \kappa\bar{G}_0\hat{c}_{ln}^{(i)}C_{lm}^{(i,3)} + [\bar{E}_2\tilde{c}_{ln}^{(i)} - ((\alpha_m^{(i)})^2\bar{G}_2 + \kappa\bar{G}_0)\tilde{c}_{ln}^{(i)}]C_{lm}^{(i,5)} - \\
&\sum_{p=0}^{M_i}\sum_{l=1}^{2}\alpha_p^{(i)}\hat{c}_{ln}^{(i)}\bar{S}_{xmp}^{(i)}[(\bar{D}_1+\bar{G}_1)\,C_{lp}^{(i,1)} + (\bar{D}_2+\bar{G}_2)C_{lp}^{(i,4)}] = -\omega^2\{I_1A_{mn}^{(i,2)} + I_2A_{mn}^{(i,5)} + \sum_{l=1}^{2}\bar{b}_{lm}^{(i)}(I_1B_{ln}^{(i,2)} + I_2B_{ln}^{(i,5)}) + \sum_{l=1}^{2}\bar{c}_{ln}^{(i)}\,(I_1C_{lm}^{(i,2)} + I_2C_{lm}^{(i,5)})\}
\end{aligned} \tag{23}$$

(m=0, 1, …,M_i and n=0, 1, …,N_i).

Similarly, satisfying the governing equations for every subdomain yields $\sum_{k=1}^{4\ \mathrm{or}\ 6} 5(M_k+1)(N_k+1)$ linear algebraic equations in total, and they can be expressed in matrix form as follows

$$(\widehat{\boldsymbol{K}}\boldsymbol{F} + \widetilde{\boldsymbol{K}}\boldsymbol{P}) = \omega^2(\widehat{\boldsymbol{M}}\boldsymbol{F} + \widetilde{\boldsymbol{M}}\boldsymbol{P}). \tag{24}$$

Substituting Eq. (20) into Eq. (24) yields

$$(\widehat{\mathbf{K}} + \widetilde{\mathbf{K}}(\mathbf{B}_{\mathrm{P}}{}^{-1}\mathbf{B}_{\mathrm{F}}))\mathbf{F} = \omega^2(\widehat{\mathbf{M}} + \widetilde{\mathbf{M}}(\mathbf{B}_{\mathrm{P}}{}^{-1}\mathbf{B}_{\mathrm{F}}))\mathbf{F}. \tag{25}$$

Eq. (25) represents a generalized eigenvalue problem, and it is solved to obtain the eigenvalues and the corresponding eigenvectors. Subsequently, the coefficient vectors **P** can be obtained using Eq. (20).

4. Convergence study and comparison

An analytical series solution is typically expected to

Table 1 Convergence of $\Omega = \omega(b^2/h)\sqrt{\rho_c/E_c}$ for FFFF side-cracked square Al/Al_2O_3 FGM plates (h/a=0.1, C_x/a=0.5, $d/b = 0.2$)

$\bar{m}$	κ	Mode	$\widetilde{M}$						Published
			15	25	35	41	45	51	
0	$\frac{\pi^2}{12}$	1	3.6085	3.6162	3.6191	3.6201	3.6206	3.6212	(3.624)
		2	5.4062	5.4093	5.4108	5.4114	5.4117	5.4120	(5.413)
		3	6.7820	6.7833	6.7843	6.7846	6.7848	6.7851	(6.786)
		4	8.8016	8.8272	8.8371	8.8406	8.8424	8.8445	(8.859)
		5	9.1048	9.1105	9.1124	9.1130	9.1133	9.1136	(9.116)
		6	13.944	14.025	14.056	14.067	14.072	14.079	/
5	$\frac{5}{6}$	1	2.3685	2.3736	2.3755	2.3761	2.3764	2.3768	{2.369}
		2	3.5376	3.5396	3.5406	3.5409	3.5411	3.5414	{3.536}
		3	4.4393	4.4402	4.4408	4.4410	4.4412	4.4413	{4.431}
		4	5.7551	5.7718	5.7783	5.7805	5.7817	5.7831	{5.760}
		5	5.9510	5.9548	5.9560	5.9564	5.9566	5.9568	{5.918}
		6	9.1098	9.1618	9.1820	9.1891	9.1927	9.1970	/

( ): Li (2009),{ }: Huang *et al.* (2013), /: no available data

Table 2 Convergence of $\Omega = \omega(b^2/h)\sqrt{\rho_c/E_c}$ for CFFF side-cracked square Al/Al_2O_3 FGM plates (h/a=0.1, C_x/a=0.5, $d/b = 0.2$)

$\bar{m}$	κ	Mode	$\widetilde{M}$						Published
			15	25	35	41	45	51	
0	$\frac{\pi^2}{12}$	1	1.0157	1.0160	1.0161	1.0161	1.0162	1.0162	(1.016) {1.017}
		2	2.3058	2.3097	2.3112	2.3117	2.3120	2.3123	(2.315) {2.322}
		3	5.6317	5.6368	5.6389	5.6396	5.6400	5.6404	(5.644) {5.655}
		4*	6.1787	6.1854	6.1882	6.1892	6.1897	6.1903	(/) {6.197}
		5	7.4385	7.4456	7.4487	7.4497	7.4503	7.4510	(7.456) {7.473}
		6	8.1330	8.1368	8.1380	8.1384	8.1386	8.1389	(8.140) {/}
5	$\frac{5}{6}$	1	0.66810	0.66825	0.66833	0.66836	0.66838	0.66840	/
		2	1.5143	1.5169	1.5178	1.5182	1.5183	1.5186	/
		3	3.6892	3.6926	3.6940	3.6945	3.6947	3.6951	/
		4*	4.0140	4.0184	4.0201	4.0208	4.0211	4.0215	/
		5	4.8682	4.8728	4.8748	4.8755	4.8758	4.8763	/
		6	5.3277	5.3301	5.3310	5.3312	5.3314	5.3315	/

( ): Li (2009),{ }: Huang *et al.* (2013), /: no available data

converge to the exact solution when the number of series terms, determined by M_i and N_i, is sufficiently large. To demonstrate the accuracy of the proposed series solutions, convergence studies of the nondimensional frequency $\Omega = \omega(b^2/h)\sqrt{\rho_c/E_c}$ of cracked plates are conducted herein. Four letters are used to denote the boundary conditions along the four edges of a rectangular plate. For example, the CFSF boundary conditions represent the clamped, free, simply supported, and free boundary conditions at x=0, y=0, x=a, and y=b, respectively. For an edge with y_i=constant in subdomain i, the S, C, and F boundary conditions are defined as follows:

Simply supported: $U_0^{(i)} = W_0^{(i)} = \Psi_x^{(i)} = N_{yy}^{(i)} = M_{yy}^{(i)} = 0$,

Clamped: $U_0^{(i)} = V_0^{(i)} = W_0^{(i)} = \Psi_x^{(i)} = \Psi_y^{(i)} = 0$, and

Free: $N_{yy}^{(i)} = N_{yy}^{(i)} = Q_y^{(i)} = M_{yy}^{(i)} = M_{xy}^{(i)} = 0$.

Similar definitions of boundary conditions can be applied to an edge with x_i=constant.

4.1 Side-cracked plates

A rectangular plate with a vertical side crack, as considered herein, is decomposed into four rectangular subdomains, and these subdomains are numbered as illustrated in Fig. 1. For simplicity, the following series solutions are obtained by setting $M_i = \widetilde{M} - 1$ for i=1-4 and

$$\frac{N_i}{M_i} = \begin{cases} 1/2 & \text{when } b_i/a_i < 0.5 \\ 1 & \text{otherwise} \end{cases}. \quad (26)$$

The relationship between M_i and N_i in Eq. (26) is applied in the present solutions.

Tables 1-3 present a summary of the convergence of the first six nondimensional frequencies Ω with increasing numbers of solution terms for the FFFF and CFFF square FGM plates with h/a=0.1 and vertical side cracks d/b=0.2 or 0.5 at C_x/a= 0.5. Six rigid-body modes corresponding to zero natural frequencies for the FFFF plate are not presented in Tables 1 and 3. In these tables, the asterisk "*" indicates that the corresponding mode is dominated by in-

Table 3 Convergence of $\Omega = \omega(b^2/h)\sqrt{\rho_c/E_c}$ for square plates with side cracks of $d/b = 0.5$ at C_x/a=0.5 (h/a=0.1)

BC	$\bar{m}$	κ	Mode	$\widetilde{M}$						Published
				15	25	35	41	45	51	
C F F F	0	$\pi^2/12$	1	0.88026	0.88130	0.88176	0.88192	0.88201	0.88212	(0.8829) [0.8853]
			2	1.7129	1.7171	1.7189	1.7195	1.7198	1.7202	(1.723) [1.729]
			3*	3.8266	3.8352	3.8389	3.8402	3.8409	3.8417	(/) [3.848]
			4	4.4661	4.4706	4.4723	4.4729	4.4732	4.4735	(4.476) [4.485]
			5	5.9313	5.9404	5.9440	5.9452	5.9459	5.9467	(5.951) [5.979]
			6	7.8664	7.8734	7.8762	7.8771	7.8776	7.8782	(7.882) [/]
F F F F	5	$5/6$	1	1.5150	1.5215	1.5241	1.5250	1.5255	1.5261	{1.525}
			2	2.6700	2.6733	2.6746	2.6750	2.6752	2.6755	{2.666}
			3	4.1039	4.1107	4.1131	4.1140	4.1144	4.1150	{4.085}
			4	4.1415	4.1467	4.1485	4.1492	4.1495	4.1499	{4.149}
			5*	4.1959	4.2022	4.2051	4.2062	4.2068	4.2075	{4.212}
			6	5.8079	5.8093	5.8095	5.8096	5.8096	5.8097	/

( ): Li (2009), [ ]: Huang *et al.* (2011b), { }: Huang *et al.* (2013), /: no available data

Table 4 Convergence of $\Omega = \omega(b^2/h)\sqrt{\rho_c/E_c}$ for SSSS square plates (h/a=0.1) with internal central cracks of $d/b = 0.2$

$\bar{m}$	κ	Mode	$\widetilde{M}$						Huang *et al.* (2011a)
			10	15	21	25	31	35	
0	$\pi^2/12$	1	5.5690	5.5723	5.5738	5.5744	5.5750	5.5753	5.577
		2	13.554	13.553	13.557	13.559	13.561	13.562	13.57
		3	13.750	13.743	13.742	13.741	13.741	13.741	13.74
		4*	19.475	19.476	19.477	19.477	19.477	19.477	/
		5*	19.484	19.483	19.483	19.483	19.483	19.483	/
		6	20.965	20.960	20.961	20.961	20.962	20.963	20.97
5	$5/6$	1	3.6564	3.6586	3.6596	3.6600	3.6604	3.6606	/
		2	8.8757	8.8753	8.8779	8.8791	8.8804	8.8810	/
		3	9.0029	8.9985	8.9976	8.9974	8.9974	8.9973	/
		4*	12.630	12.631	12.631	12.631	12.632	12.632	/
		5*	12.638	12.638	12.638	12.638	12.638	12.638	/
		6	13.697	13.694	13.695	13.695	13.696	13.696	/

/: no available data

plane deformation. Notably, when $\bar{m} = 0$, the asterisk "*" indicates that the mode is a pure in-plane mode and corresponds to $u_0^{(i)}$ or $v_0^{(i)}$. To compare the results obtained herein with those derived by existing FSDT-based studies, the transverse shear correction coefficient κ was set to $\pi^2/12$ for homogeneous plates ($\bar{m} = 0$).

Notably, all the Ω values presented in these tables converge from the lower bounds when the number of solution terms increases. According to Table 1, the relative differences between the results obtained by setting $\widetilde{M}$ to 51 and those obtained by setting $\widetilde{M}$ to 35 and 45 are less than 0.2% and 0.05%, respectively. Similarly, as indicated in Table 2, the relative differences are less than 0.06% and 0.035%, as listed in Table 3, the relative differences are less than 0.08% and 0.02% for the CFFF plate and less than 0.15% and 0.04% for the FFFF plate.

For comparison, these tables also present the results obtained by Li (2009), Huang *et al.* (2011b), and Huang *et al.* (2013) on the basis of FSDT, Reddy's TSDT, and three-dimensional elasticity, respectively. These results were obtained by integrating the Ritz method with admissible functions, including appropriate crack functions, which accurately describe the stress singularities at the tip of the crack and display displacement and slope discontinuities across the crack. Li (2009) studied the vibrations of homogeneous plates but did not consider the in-plane deformations on the middle plane of a plate. Notably, the Ritz method yields upper-bound solutions for natural frequencies. The FSDT-based results obtained in the present study using $\widetilde{M}$=51 are in excellent agreement with those obtained by Li (2009), and the results obtained in the present study are smaller than those obtained by Li by less than 0.2%. The exact Ω values should lie between the values obtained herein and those reported by Li (2009). Additionally, the results obtained herein by setting $\widetilde{M}$ to 51 are in good agreement with those obtained using Reddy's TSDT and three-dimensional elasticity.

4.2 Internally cracked plates

A rectangular plate with an internal vertical crack is decomposed into six rectangular subdomains, which are

Table 5 Convergence of $\Omega = \omega(b^2/h)\sqrt{\rho_c/E_c}$ for square FGM plates ($\bar{m} = 5$, h/a=0.1) with internal central cracks of $d/b = 0.5$

BC	Mode	$\widetilde{M}$						Huang *et al.* (2012)
		15	25	31	35	41	45	
SSSS	1	3.3169	3.3188	3.3192	3.3194	3.3198	3.3199	/
	2	7.1381	7.1766	7.1851	7.1898	7.1956	7.1982	/
	3	8.8366	8.8373	8.8376	8.8378	8.8381	8.8382	/
	4*	12.452	12.458	12.460	12.461	12.462	12.462	/
	5*	12.638	12.638	12.638	12.638	12.638	12.638	/
	6*	12.804	12.831	12.836	12.839	12.843	12.845	/
CFFF	1	0.64100	0.64139	0.64147	0.64152	0.64158	0.64161	0.6423
	2	1.5677	1.5686	1.5687	1.5688	1.5689	1.5689	1.561
	3	3.3679	3.3730	3.3738	3.3744	3.3751	3.3754	3.365
	4*	3.9326	3.9389	3.9406	3.9414	3.9424	3.9428	3.960
	5	4.8251	4.8266	4.8271	4.8274	4.8277	4.8279	4.808
	6	5.5006	5.5035	5.5040	5.5042	5.5045	5.5046	/
SFSF	1	1.5408	1.5433	1.5437	1.5440	1.5444	1.5445	/
	2	3.0212	3.0225	3.0226	3.0227	3.0228	3.0228	/
	3	6.3732	6.3742	6.3744	6.3745	6.3746	6.3747	/
	4	6.3950	6.4164	6.4210	6.4237	6.4269	6.4283	/
	5	8.3219	8.3245	8.3250	8.3253	8.3258	8.3259	/
	6*	9.4858	9.4875	9.4878	9.4880	9.4882	9.4883	/

/: no available data

Table 6 $\Omega = \omega(b^2/h)\sqrt{\rho_c/E_c}$ for SSSS square plates with side cracks at C_x/a=0.5

h/b	$\bar{m}$	*d/b*	Mode					
			1	2	3	4	5	6
0.02	0	0	5.9717	14.903	14.903	23.783	29.710	29.710
		0.2	5.9517	14.831	14.861	23.664	29.372	29.672
		0.5	5.6090	12.896	14.431	19.297	26.290	29.307
	5	0	3.9300	9.8058	9.8058	15.646	19.543	19.543
		0.2	3.9169	9.7588	9.7783	15.568	19.321	19.518
		0.5	3.6913	8.4846	9.4952	12.695	17.292	19.278
0.1	0	0	5.7670	13.765	13.765	19.483*	19.483*	21.122
		0.2	5.7497 [5.750] (5.758)	13.672 [13.68] (13.72)	13.698 [13.70] (13.74)	18.534* [18.56] (18.57)	19.483* [19.48] (19.48)	20.885 [/] (/)
		0.5	5.3763 (5.385)	11.319 (11.40)	13.319 (13.35)	16.172* (16.19)	17.278 (17.35)	19.483* (/)
	0.5	0	4.8993	11.726	11.726	17.484*	17.484*	18.042
		0.2	4.8825	11.650	11.669	16.633*	17.484*	17.847
		0.5	4.5668	9.6793	11.345	14.499*	14.757	17.484*
	5	0	3.7872	9.0060	9.0060	12.638*	12.638*	13.785
		0.2	3.7740 [3.756] (3.759)	8.9447 [8.851] (8.867)	8.9620 [8.867] (8.885)	12.023* [12.04] (12.05)	12.638* [12.64] (12.64)	13.631 [/] (/)
		0.5	3.5283	7.4079	8.7118	10.481*	11.293	12.638*

( ): Huang *et al.* (2013), [ ]: Huang *et al.* (2011b), /: no available data

numbered as illustrated in Fig. 1. For simplicity, the following solutions for the vibrations of a plate with a vertical central crack were obtained by setting M_i+1=$\widetilde{M}$ for i=1-6, and N_i was determined using Eq. (26).

Table 4 lists the nondimensional frequencies Ω of the first six modes for the SSSS square plates (h/a=0.1) with vertical central cracks of d/b=0.2, these frequencies were obtained by setting $\widetilde{M}$ to 10, 15, 25, 31, and 35. The frequencies converge from the lower bounds when the number of series solution terms increases gradually from $\widetilde{M}$=15 to $\widetilde{M}$=35, except for the Ω values for the third modes of the FGM plates with $\bar{m} = 0$ and 5. The frequencies of these modes converge from the upper bounds. The relative differences between the frequencies obtained by setting $\widetilde{M}$ to 35 and those obtained by setting $\widetilde{M}$ to 21 and 31 are smaller than 0.04% and 0.008%, respectively. Furthermore,

Table 7 $\Omega = \omega(b^2/h)\sqrt{\rho_c/E_c}$ for SFSF rectangular plates with side cracks at C_x/a=0.5

a/b	*h/b*	$\bar{m}$	*d/b*	Mode					
				1	2	3	4	5	6
1	0.02	0	0	2.9174	4.8548	11.013	11.768	14.071	21.177
			0.2	2.7350	4.6841	10.943	10.977	12.977	19.188
			0.5	2.1218	4.5322	5.1700	10.844	12.473	17.925
		5	0	1.9200	3.1949	7.2462	7.7437	9.2581	13.931
			0.2	1.8000	3.0825	7.2003	7.2222	8.5381	12.622
			0.5	1.3963	2.9826	3.4016	7.1351	8.2076	11.792
	0.1	0	0	2.8572	4.6567	10.245	11.003	12.950	14.755*
			0.2	2.6493	4.4729	9.7957	10.201	11.908	12.037*
			0.5	2.0219	4.3465	4.6154	5.9332*	10.048	11.565
		0.5	0	2.4234	3.9546	8.7116	9.3645	11.030	13.239*
			0.2	2.2484	3.7989	8.3642	8.6735	10.143	10.803*
			0.5	1.7172	3.6908	3.9393	5.3256	8.5443	9.8475
		5	0	1.8778	3.0554	6.6947	7.2055	8.4690	9.5681*
			0.2	1.7409	2.9347	6.4115	6.6659	7.7906	7.8111*
			0.5	1.3281	2.8520	3.0265	3.8532*	6.5656	7.5677
2	0.1	0	0	0.71577	2.0017	2.8582	4.6574	5.3885*	6.3399
			0.2	0.69033	1.9849	2.8233	4.4671	4.7023*	6.0990
			0.5	0.59562	1.9603	2.3331	2.7514*	3.6614	5.4285
		5	0	0.47093	1.3145	1.8785	3.0558	3.5018*	4.1598
			0.2	0.45416	1.3034	1.8555	2.9309	3.0560*	4.0013
			0.5	0.39178	1.2867	1.5328	1.7887*	2.4035	3.5605
	0.2	0	0	0.70560	1.8857	2.6942*	2.7188	4.2651	5.7466
			0.2	0.67746	1.8696	2.3512*	2.6744	4.0753	5.5288
			0.5	0.57804	1.3757*	1.8473	2.1342	3.3933	4.9422
		5	0	0.46375	1.2284	1.7594*	1.7803	2.7767	3.7467
			0.2	0.44520	1.2156	1.5382*	1.7512	2.6534	3.6028
			0.5	0.37975	0.89105*	1.2126	1.3972	2.2131	3.2116

the frequencies obtained by setting $\widetilde{M}$ to 35 show excellent agreement with those reported by Huang *et al.* (2011a), and the differences are smaller than 0.06%. Notably, on the basis of FSDT, Huang *et al.* (2011a) determined the frequencies of cracked homogeneous plates by using the Ritz method with admissible functions including crack functions, which accurately describe the stress singularities at the tips of the crack and display displacement and slope discontinuities across the crack, and claimed their results accurate to at least three significant figures.

Table 5 lists the nondimensional frequencies Ω of the SSSS, CFFF, and SFSF square FGM plates (h/a=0.1, $\bar{m}$ = 5) with vertical central cracks of d/b=0.5, these frequencies were obtained by setting $\widetilde{M}$ to 15, 25, 31, 35, 41, and 45. These frequencies converge from the lower bounds. The frequencies computed by setting $\widetilde{M}$ to 31 and 41 are smaller than those computed by setting $\widetilde{M}$ to 45 by less than 0.2% and 0.04%, respectively, for the SSSS plate, less than 0.06% and 0.01%, respectively, for the CFFF plate, and less than 0.2% and 0.03%, respectively, for the SFSF plate. The frequencies of the CFFF plate obtained by setting $\widetilde{M}$ to 45 agree well with those determined using the Ritz method on the basis of three-dimensional elasticity (Huang *et al.* 2012), and the relative differences are smaller than 0.5%.

5. Numerical results

After the verification of accuracy of the proposed solutions through comprehensive convergence studies, this paper presents an extensive tabulation of the results of the first six nondimensional frequency parameters for the rectangular plates with side and internal vertical cracks under various boundary condition combinations, the purpose of the tabulation is to provide a database for comparison with frequencies obtained using various numerical solutions. In the subsequent tables, the frequencies of the intact plates were obtained without dividing the plates into several subdomains. The frequencies of the FFFF intact plates were determined by setting $\widetilde{M}$ to 45, and those of the plates under other boundary condition combinations were obtained by setting $\widetilde{M}$ to 35.

Tables 6-8 present a summary of the first six nondimensional frequencies Ω of the SSSS, SFSF, CFFF, and CFCF rectangular plates (a/b=1 and 2, $\bar{m}$ = 0, 0.5, and 5) with various thickness-width ratios (h/b=0.02, 0.1, and 0.2) and vertical side cracks (d/b=0.2 and 0.5) at C_x/a=0.5. Tables 9 and 10 list the Ω values of for the first six modes of the SSSS, SFSF, FFFF, CFFF and CFSF rectangular

Table 8 $\Omega = \omega(b^2/h)\sqrt{\rho_c/E_c}$ for CFFF and CFCF rectangular plates with side cracks at C_x/a=0.5

BC	*a*/*b*	*h*/*b*	$\bar{m}$	*d*/*b*	Mode					
					1	2	3	4	5	6
CFFF	2	0.02	0	0	0.26005	1.1120	1.6200	3.6176	4.5411	6.9441
				0.2	0.25843	1.0833	1.5713	3.5459	4.4901	6.6770
				0.5	0.24662	0.93405	1.3881	3.0958	3.8618	5.5659
			5	0	0.17116	0.73185	1.0662	2.3807	2.9886	4.5696
				0.2	0.17010	0.71290	1.0342	2.3335	2.9548	4.3937
				0.5	0.16232	0.61470	0.91355	2.0373	2.5414	3.6627
		0.1	0	0	0.25889	1.0729	1.5954	2.1725*	3.4590	4.3896
				0.2	0.25644 {0.2565}	1.0455 {1.047}	1.5390 {1.540}	2.0878* {/}	3.3836 {3.386}	4.3121 {4.315}
				0.5	0.24347 {0.2435}	0.89795 {0.8995}	1.3470 {1.347}	1.5999* {/}	2.9123 {2.919}	3.6504 {3.653}
			5	0	0.17037	0.70451	1.0488	1.4126*	2.2701	2.8808
				0.2	0.16875	0.68652	1.0116	1.3575*	2.2206	2.8298
				0.5	0.16019	0.58956	0.88527	1.0403*	1.9112	2.3956
		0.2	0	0	0.25655	1.0037	1.0863*	1.5303	3.1627	3.9434*
				0.2	0.25367	0.97914	1.0439*	1.4710	3.0914	3.5124*
				0.5	0.23917	0.79929*	0.83853	1.2794	2.2645*	2.6076
			5	0	0.16873	0.64410	0.72101*	1.0025	2.0585	2.5457*
				0.2	0.16683	0.62665	0.69476*	0.96354	2.0098	2.2863*
				0.5	0.15726	0.50861*	0.56113	0.83763	1.4691*	1.7085
CFCF	1	0.02	0	0	6.6820	7.9316	13.047	18.367	20.118	23.874
				0.2	6.3417	7.6447	12.960	15.724	18.994	23.873
				0.5	5.3679	7.4865	7.5279	12.754	18.707	21.966
			5	0	4.3975	5.2195	8.5842	12.084	13.236	15.703
				0.2	4.1733	5.0305	8.5269	10.343	12.496	15.702
				0.5	3.5324	4.9256	4.9538	8.3911	12.307	14.448
		0.1	0	0	6.2421	7.2677	11.662	15.944	17.262	17.745*
				0.2	5.8907	7.0075	11.586	12.985	16.394	17.216*
				0.5	5.0352	6.6615	6.9299	11.378	15.959	17.032*
			5	0	4.0971	4.7623	7.6137	10.424	11.272	11.483*
				0.2	3.8657	4.5925	7.5640	8.4830	10.712	11.145*
				0.5	3.3038	4.3640	4.5425	7.4282	10.420	11.013*
	2	0.1	0	0	1.6322	2.5819	4.4004	5.8202	7.7732	7.9170*
				0.2	1.5903 (1.598)	2.5502 (2.560)	4.3298 (4.355)	5.5572 (5.592)	7.6329* (7.654)	7.7661 (/)
				0.5	1.4465 (1.453)	2.5127 (2.521)	3.1694 (3.197)	4.8927 (4.915)	7.1688 (7.206)	7.2784* (/)
			5	0	1.0735	1.6949	2.8900	3.8164	5.0835	5.1441*
				0.2	1.0458	1.6741	2.8435	3.6438	4.9591*	5.0791
				0.5	0.95116	1.6495	2.0807	3.2105	4.6776	4.7470*

{ }: Huang *et al.* (2011a), ( ): Huang *et al.* (2013)

plates with internal vertical central cracks (*d*/*b*=0.2 and 0.5). The frequency parameters of the SFSF and CFCF side-cracked plates were obtained by setting $\widetilde{M}$ to 51, and those of the side-cracked plates under other boundary conditions and *d*/*b*=0.2 and 0.5 were obtained by setting $\widetilde{M}$ to 31 and 45, respectively. The nondimensional frequencies of the square plates with internal cracks of *d*/*b*=0.2 were determined by setting $\widetilde{M}$ to 35, and those of the other plates were found by setting $\widetilde{M}$ to 45. The solutions obtained using the various $\widetilde{M}$ values are accurate to at least three significant figures. As listed in Table 8, almost all solutions obtained for the CFFF rectangular homogeneous plates with *a*/*b*=2, *h*/*b*=0.1, and *d*/*b*=0.2 and 0.5 are consistent (up to three significant figures) with those obtained by Huang *et al.* (2011a) using the Ritz method. Notably, κ=5/6 and $\pi^2/12$ were adopted in the present solutions and those of Huang *et al.* (2011a), respectively. Tables 6 and 8 also show the published results obtained for the SSSS and CFCF plates through the Ritz method, based on Reddy's TSDT (Huang *et al.*, 2011b) and three-dimensional elasticity (Huang *et al.*, 2013). The results obtained herein agree well with those reported in the literature.

Fig. 2 displays the mode shapes of the side-cracked SSSS, SFSF, CFFF, and CFCF square plates with $\bar{m}=5$, *h*/*b*=0.1, and vertical cracks of *d*/*b*=0.2 at C_x/a=0.5, while Fig. 3 depicts the mode shapes of the SFSF, FFFF, CFFF,

Table 9 $\Omega = \omega(b^2/h)\sqrt{\rho_c/E_c}$ for SSSS and SFSF rectangular plates with internal vertical central cracks

BC	*a*/*b*	*h*/*b*	$\bar{m}$	*d*/*b*	Mode 1	2	3	4	5	6
SSSS	2	0.02	0	0	3.7365	5.9773	9.7165	12.680	14.905	14.940
				0.2	3.7085	5.9630	9.4980	12.663	14.854	14.881
				0.5	3.6243	5.8177	8.8916	12.595	13.628	14.824
			5	0	2.4591	3.9337	6.3938	8.3439	9.8073	9.8300
				0.2	2.4407	3.9243	6.2502	8.3326	9.7737	9.7913
				0.5	2.3853	3.8286	5.8510	8.2876	8.9662	9.7542
		0.1	0	0	3.6521	5.7702	9.1899	9.7417*	11.832	13.765
				0.2	3.6222	5.7574	8.9673	9.7417*	11.828	13.665
				0.5	3.5299	5.5602	8.3686	9.7417*	11.762	12.011
			5	0	2.3995	3.7875	6.0233	6.3244*	7.7470	9.0062
				0.2	2.3798	3.7791	5.8769	6.3244*	7.7443	8.9410
				0.5	2.3190	3.6496	5.4830	6.3244*	7.7006	7.8595
SFSF	1	0.02	0	0	2.9174	4.8548	11.013	11.768	14.071	21.177
				0.2	2.8266	4.8553	10.888	11.730	14.050	21.082
				0.5	2.4668	4.8150	10.549	11.005	13.987	18.109
			5	0	1.9200	3.1949	7.2462	7.7437	9.2581	13.931
				0.2	1.8603	3.1952	7.1636	7.7187	9.2444	13.869
				0.5	1.6233	3.1686	6.9405	7.2408	9.2026	11.912
		0.1	0	0	2.8572	4.6567	10.245	11.003	12.950	14.755*
				0.2	2.7478	4.6553	10.082	10.937	12.903	14.752*
				0.5	2.3510	4.6072	9.7569	9.8131	12.733	14.633*
			5	0	1.8778	3.0554	6.6947	7.2055	8.4690	9.5681*
				0.2	1.8057	3.0544	6.5881	7.1623	8.4383	9.5664*
				0.5	1.5445	3.0228	6.3747	6.4283	8.3259	9.4883*
	2	0.02	0	0	0.72411	2.0679	2.9286	4.8616	6.6311	7.9395
				0.2	0.70873	2.0687	2.9138	4.8520	6.4918	7.9126
				0.5	0.65774	2.0658	2.8991	4.8447	6.0644	7.8553
			5	0	0.47656	1.3609	1.9273	3.1993	4.3635	5.2243
				0.2	0.46646	1.3614	1.9177	3.1930	4.2722	5.2066
				0.5	0.43289	1.3595	1.9080	3.1882	3.9907	5.1688
		0.1	0	0	0.71577	2.0017	2.8582	4.6574	5.3885*	6.3399
				0.2	0.70098	2.0016	2.8549	4.6393	5.3870*	6.2165
				0.5	0.64206	1.9980	2.8274	4.6032	5.3302*	5.7689
			5	0	0.47093	1.3145	1.8785	3.0558	3.5018*	4.1598
				0.2	0.46117	1.3145	1.8763	3.0438	3.5008*	4.0787
				0.5	0.42233	1.3120	1.8581	3.0198	3.4639*	3.7840

Table 10 $\Omega = \omega(b^2/h)\sqrt{\rho_c/E_c}$ for CFFF and CFCF rectangular plates with internal vertical central cracks

BC	*a*/*b*	*h*/*b*	$\bar{m}$	*d*/*b*	Mode 1	2	3	4	5	6
FFFF	1	0.02	5	0	2.6570	3.9319	4.8432	6.8694	6.8694	12.109
				0.2	2.6527	3.8439	4.6880	6.8541	6.8573	12.062
				0.5	2.6448	3.4407	4.3759	6.6088	6.7672	10.524
		0.1		0	2.5250	3.7522	4.6206	6.3115	6.3115	10.914
				0.2	2.5037	3.6814	4.4560	6.2984	6.3075	10.753
				0.5	2.4634	3.2096	4.1706	6.0047	6.2028	8.7660
	2			0	1.0578	1.2666	2.7528	2.8752	4.2006	4.7000
				0.2	1.0300	1.2603	2.7526	2.8719	4.1776	4.6891
				0.5	0.92549	1.2483	2.7409	2.8301	4.0957	4.6608
CFFF	1	0.02	5	0	0.69070	1.6798	4.2237	5.3825	6.1018	10.634
				0.2	0.68584	1.6795	4.1202	5.3357	6.1072	10.503
				0.5	0.65776	1.6750	3.6536	5.1743	6.0349	9.9136
	2	0.1		0	0.25889	1.0729	1.5954	2.1725*	3.4590	4.3896
				0.2	0.25760	1.0691	1.5636	2.1660*	3.4564	4.3849
				0.5	0.25152	1.0615	1.4393	2.1249	3.4399	4.3203
			5	0	0.17037	0.70451	1.0488	1.4126*	2.2701	2.8808
				0.2	0.16951	0.70198	1.0278	1.4083*	2.2684	2.8777
				0.5	0.16550	0.69689	0.94595	1.3817*	2.2575	2.8353
CFSF	1	0.02	5	0	3.0215	4.0740	7.8334	9.8015	11.121	15.229
				0.2	2.9590	4.0740	7.7300	9.7437	11.112	15.230
				0.5	2.7026	4.0386	7.4580	8.9019	11.041	13.050
		0.1		0	2.8901	3.8163	7.1099	8.7964	9.8319	10.098*
				0.2	2.8162	3.8139	6.9857	8.7177	9.8029	9.8699*
				0.5	2.5420	3.7721	6.7429	7.6110	8.0959*	9.6679
	2	0.02	5	0	1.1247	2.2628	3.5969	5.2047	6.6035*	7.3482
				0.2	1.1093	2.2623	3.5846	5.1865	6.5929*	7.2178
				0.5	1.0482	2.2567	3.5135	5.1469	6.5056*	6.7068
		0.1		0	0.73985	1.4857	2.3632	3.4139	4.2911*	4.8193
				0.2	0.72964	1.4854	2.3551	3.4018	4.2842*	4.7333
				0.5	0.68941	1.4817	2.3082	3.3755	4.2274*	4.3964

and CFSF square plates with vertical internal central cracks. In these figures, the out-of-plane displacement contours (solid lines) and nodal lines (dashed lines) represent the modes dominated by out-of-plane displacement. Moreover, blank mode shapes show the in-plane mode deformations and represent the modes dominated by in-plane displacements.

On the basis of the results presented in Tables 6-10 and Figs. 2 and 3, the following inferences are drawn:

1. When $\bar{m} = 0$ changes to $\bar{m} = 0.5$ and then to $\bar{m} = 5$, *a*/*b* changes from 1 to 2, or *d*/*b* changes from 0 to 0.2 and then to 0.5, the frequencies decrease because of the decrease in plate stiffness.

2. When *d*/*b* increases from 0 to 0.2, the frequencies of the side-cracked thin plates with *h*/*b*=0.02 decrease by less than 1%, 4%, 10% and 15% under the SSSS, CFFF, SFSF, and CFCF boundary conditions, respectively. For the side-cracked square plates with *h*/*b*=0.1, such change in *d*/*b* declines Ω by less than 2%, 8% and 19% for the out-of-plane-displacement-dominated modes of the SSSS, SFSF, and CFCF plates, respectively. For the rectangular plates with *a*/*b*=2 and *h*/*b*=0.1, the increase in *d*/*b* leads to a less than 5% decrease in the frequencies of the out-of-plane-displacement-dominated modes of the SFSF, CFFF, and CFCF plates.

3. The frequencies of the internally cracked SSSS, SFSF, FFFF, CFFF, and CFSF plates with *d*/*b*=0.2 are smaller than those of the intact plates by less than 4%.

4. Let Δ_j denote the ratio of the frequency of mode *j* of a cracked plate to that of an intact plate. Although the Δ_j values depend on mode number, boundary conditions, plate geometries, and crack configurations, the Δ_j values of the homogenous plates are slightly different from those of the FGM plates with $\bar{m} = 5$. The differences are smaller than 1% for most of the results of the side-cracked plates and smaller than 0.2% for the internally cracked plates.

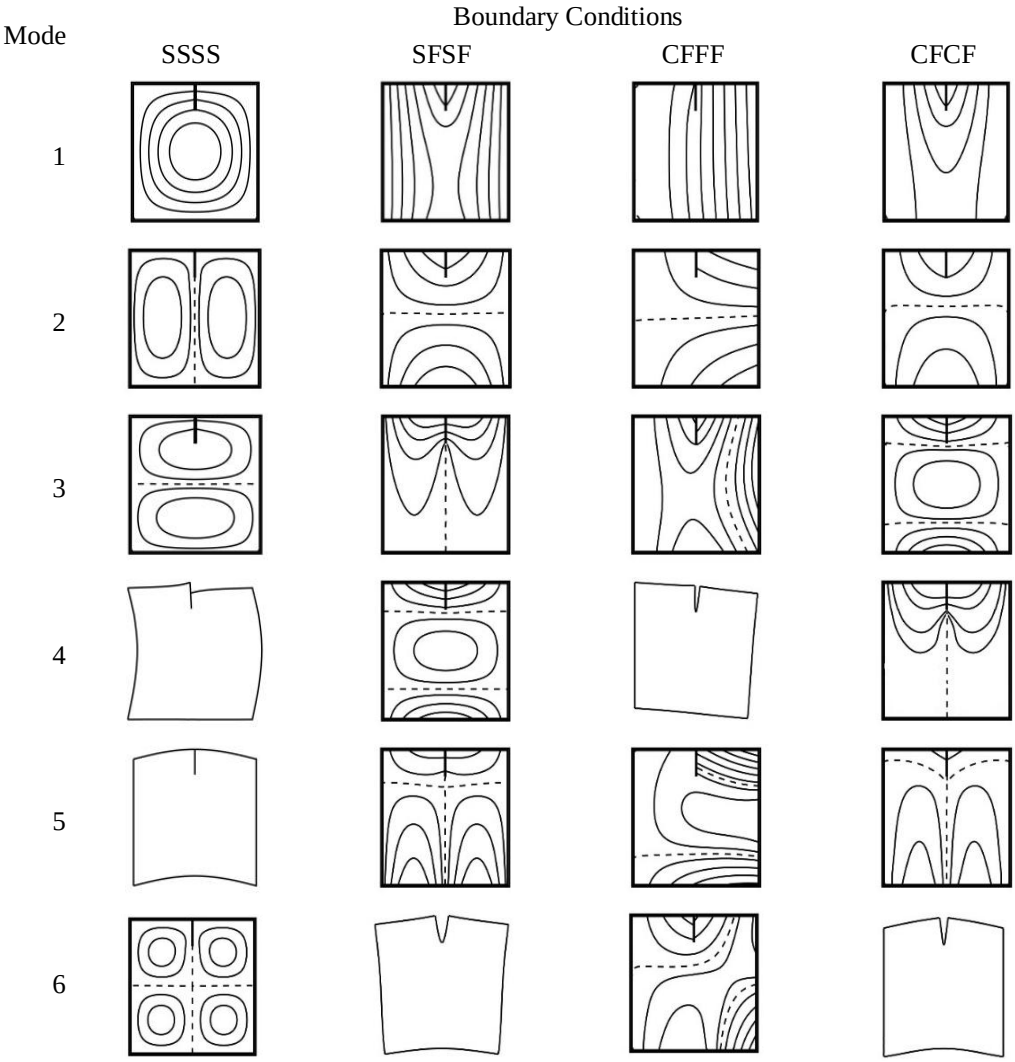

Fig. 2 The first six modal shapes of FGM square plates (h/b=0.1, $\bar{m}=5$) with vertical side cracks of d/b=0.2 at C_x/a=0.5

5. A notable observation for the data in Table 6 is that crack length does not affect the Ω values (Ω= 19.483, 17.484 and 12.638) for the side-cracked SSSS square plates with $\bar{m}=0$, 0.5, and 5, respectively. The modes corresponding to these frequencies are in-plane modes (see the fifth mode in Fig. 2). These modes correspond to the exact closed-form Navier solutions for the vibrations of intact SSSS square plates with wave numbers of 1 and 0 in the x and y directions, respectively. Such solutions result in zero stress resultants $N_{xx}, N_{xy}, Q_x, M_{xx}$ and M_{xy} along x/a=0.5.

6. As expected, the mode shapes of the side-cracked SSSS, SFSF, and CFCF square plates (Fig. 2) are symmetrical or anti-symmetrical about x/a=0.5. The side crack destroys the symmetry of the mode shapes of these plates about y/b=0.5. The mode shapes of internally cracked SFSF and FFFF square plates (Fig. 3) have two axes of symmetry, while those of the CFFF and CFSF plates have one axis of symmetry along y/b=0.5.

5. Conclusions

On the basis of FSDT, this study presented analytical series solutions for the vibrations of rectangular FGM plates with cracks parallel to an edge of the plates. Side-cracked and internally cracked plates are decomposed into four and six rectangular subdomains, respectively. The five displacement functions in each subdomain are expressed in terms of Fourier cosine series and polynomial auxiliary functions. The desired analytical solutions are established by satisfying the governing equations in each domain, boundary conditions along the crack and the four edges, and continuity conditions between two adjacent subdomains without an approximation.

The accuracy of the proposed analytical solutions was confirmed through comprehensive convergence studies of the natural frequencies of the side-cracked FFFF and CFFF square plates and internally cracked SSSS, CFFF, and SFSF square plates. Most of the results converge from the lower bounds. The well-converged results obtained herein for homogeneous plates are in excellent agreement with

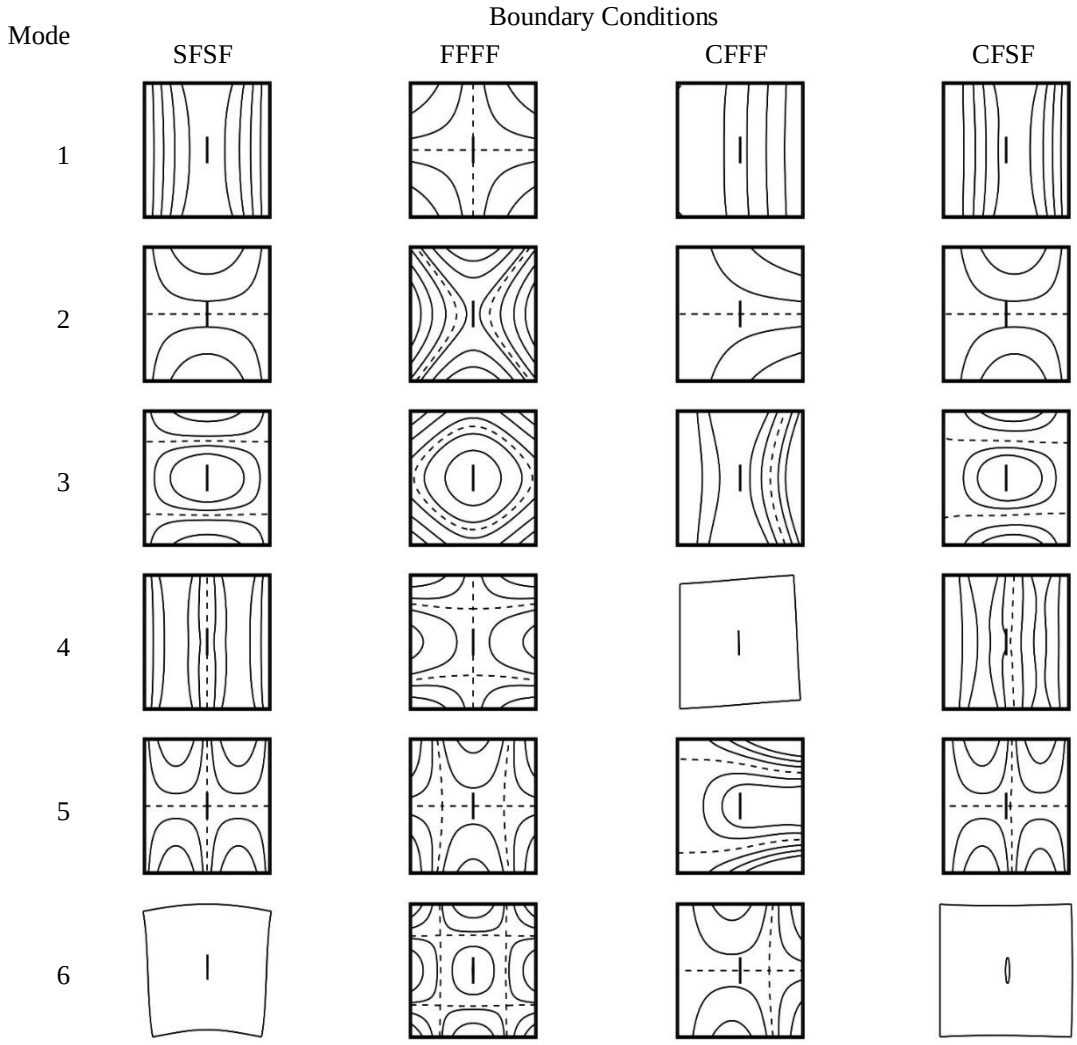

Fig. 3 The first six mode shapes of FGM square plates (h/b=0.1, $\bar{m} = 5$) with internal vertical central cracks of d/b=0.2

literature results obtained using the Ritz method on the basis of FSDT. The results obtained herein for FGM plates are also in close agreement with literature results obtained on the basis of Reddy's TSDT and three-dimensional elasticity.

Accurate nondimensional frequency data were provided for the cracked rectangular Al/Al_2O_3 FGM plates with a/b=1 and 2, h/b=0.02 and 0.1, $\bar{m} = 0$, 0.5 and 5, and d/b=0, 0.2, and 0.5 under six boundary condition combinations (SSSS, SFSF, FFFF, CFFF, CFSF and CFCF). Increasing the crack length or $\bar{m}$ reduces the non-dimensional frequencies of the cracked plates because of the decrease in plate stiffness. The frequencies of the internally cracked plates with d/b=0.2 are smaller than those of the intact plates by less than 4%, while the decreases in frequencies of the side-cracked CFCF square plates with h/b=0.05 and 0.1 can reach up to 15% and 19%, respectively. These frequencies can be used as benchmark data for assessing the accuracy of numerical approaches based on FSDT.

Unlike typical numerical methods, the approach used herein is not applicable for establishing analytical solutions for vibrations of plates with complicated geometries and cracks with arbitrary configurations. However, in theory, the present approach can be extended to develop analytical solutions for vibrations of a plate that can be decomposed into rectangular subdomains.

Acknowledgments

This work reported herein was supported by the Ministry of Science and Technology, Taiwan through research grant no. MOST 109-2221-E-009-001-MY2 and MOST 111-2221-E-A49-015-MY2. This support is gratefully acknowledged.

References

Aggarwala, B.D. and Ariel, P.D. (1981), "Vibration and bending of a cracked plate", *Rozprawy Inzynierskie*, **29**(2), 295-310.

Azam, M.S., Ranjan, V. and Kumar, B. (2017), "Free vibration analysis of rhombic plate with central crack", *Int. J. Acoust. Vib.*, **22**(4), 481-492. https://doi.org/10.20855/ijav.2017.22.4494.

Bachene, M., Tiberkak, R. and Rechak, S. (2009), "Vibration analysis of cracked plates using the extended finite element

method", *Arch. Appl. Mech.*, **79**, 249-262. https://doi.org/10.1007/s00419-008-0224-7.

Doan, D.H., Do, T.V., Pham, P.M. and Duc, N.D. (2019), "Validation simulation for free vibration and buckling of cracked Mindlin plates using phase field method", *Mech. Adv. Mater. Struct.*, **26**(12), 1018-1027. https://doi.org/10.1080/15376494.2018.1430262.

Duc, N.D. and Minh, P.P. (2021), "Free vibration analysis of cracked FG CNTRC plates using phase field theory", *Aerosp. Sci. Technol.*, **112**, 106654. https://doi.org/10.1016/j.ast.2021.106654.

Fantuzzi, N., Tornabene, F. and Viola, E. (2015), "Four-parameter functionally graded cracked plates of arbitrary shape: A GDQFEM solution for free vibrations", *Mech. Adv. Mater. Struct.*, **23**(1), 89-107. https://doi.org/10.1080/15376494.2014.933992.

Gayen, D., Tiwari, R. and Chakraborty, D. (2019), "Static and dynamic analyses of cracked functionally graded structural components: A review", *Compos. Part B-Eng.*, **173**, 106982. https://doi.org/10.1016/j.compositesb.2019.106982.

Hosseini-Hashemi, S., Gh, H.R. and Rokni, H.D.T. (2010), "Exact free vibration of rectangular Mindlin plates with all-over part-through open cracks", *Compos. Struct.*, **88**, 1015-1032. https://doi.org/10.1016/j.compstruc.2010.06.004.

Huang, C.S. and Leissa, A.W. (2009), "Vibration analysis of rectangular plates with side cracks via the Ritz method", *J. Sound Vib.*, **323**, 974-988. https://doi.org/10.1016/j.jsv.2009.01.018.

Huang, C.S., Lee, H.T., Li, P.Y. and Chang, M.J. (2021), "Three-dimensional free vibration analyses of preloaded cracked plates of functionally graded materials via the MLS-Ritz method", *Mater.*, **14**, 7712. https://doi.org/10.3390/ma14247712.

Huang, C.S., Leissa, A.W. and Li, R.S. (2011a), "Accurate vibration analysis of thick, cracked rectangular plates", *J. Sound Vib.*, **330**, 2079-2093. https://doi.org/10.1016/j.jsv.2010.11.007.

Huang, C.S., McGee, O.G. and Chang, M.J. (2011b), "Vibrations of cracked rectangular FGM thick plates", *Compos. Struct.*, **93**(7), 1747-1764. https://doi.org/10.1016/j.compstruct.2011.01.005.

Huang, C.S., McGee, O.G. and Wang, K.P. (2013), "Three-dimensional vibrations of cracked rectangular parallelepipeds of functionally graded material", *Int. J. Mech. Sci.*, **70**, 1-25. https://doi.org/10.1016/j.ijmecsci.2012.05.009.

Huang, C.S., Yang, P.J. and Chang, M.J. (2012), "Three-dimensional vibrations of functionally graded material cracked rectangular plates with through internal cracks", *Compos. Struct.*, **94**(9), 2764-2776. https://doi.org/10.1016/j.compstruct.2012.04.003.

Joshi, P.V., Jain, N.K. and Ramtekkar, G.D. (2015), "Analytical modeling for vibration analysis of thin rectangular orthotropic/functionally graded plates with an internal crack", *J. Sound Vib.*, **344**, 377-398. https://doi.org/10.1016/j.jsv.2015.01.026.

Khalafia, V. and Fazilati, J. (2021), "Free vibration analysis of functionally graded plates containing embedded curved cracks", *Struct. Eng. Mech.*, **79**(2), 157-168. https://doi.org/10.12989/sem.2021.79.2.157.

Lee, H.P. and Lim, S.P. (1993), "Vibration of cracked rectangular plates including transverse shear deformation and rotary inertia", *Comput. Struct.*, **49**(4), 715-718. https://doi.org/10.1016/0045-7949(93)90074-N.

Li, R.S. (2009), "Vibrations of rectangular cracked Mindlin plates via the Ritz", M.S. Thesis, National Chiao Tung University, Hsinchu, Taiwan.

Li, W.L. (2000), "Free vibrations of beams with general boundary conditions", *J. Sound Vib.*, **237**(4), 709-725. https://doi.org/10.1006/jsvi.2000.3150.

Li, W.L., Zhang, X., Du, J. and Liu, Z. (2009), "An exact series solution for the transverse vibration of rectangular plates with general elastic boundary supports", *J. Sound Vib.*, **321**, 254-269. https://doi.org/10.1016/j.jsv.2008.09.035.

Liew, K.M., Hung, K.C. and Lim, M.K. (1994), "A solution method for analysis of cracked plates under vibration", *Eng. Fract. Mech.*, **48**(3), 393-404. https://doi.org/10.1016/0013-7944(94)90130-9.

Liu, F.L. and Liew, K. (1999), "Vibration analysis of discontinuous Mindlin plates by differential quadrature element method", *J. Vib. Acoust.*, **121**, 204-208. https://doi.org/10.1115/1.2893965.

Lynn, P.P. and Kumbasar, N. (1967), "Free vibrations of thin rectangular plates having narrow cracks with simply supported edges", *Develop. Mech.*, **4**, 911-928.

Mindlin, R.D. (1951), "Influence of rotary inertia and shear on flexural motions of isotropic elastic plates", *J. Appl. Mech.*, ASME, **18**(1), 31-38. https://doi.org/10.1115/1.4010217.

Minh, P.P. and Duc, N.D. (2021), "The effect of cracks and thermal environment on free vibration of FGM plates", *Thin Wall. Struct.*, **159**, 107291. https://doi.org/10.1016/j.tws.2020.107291.

Minh, P.P., Manh, D.T. and Duc, N.D. (2021), "Free vibration of cracked FGM plates with variable thickness resting on elastic foundations", *Thin Wall. Struct.*, **161**, 107425, https://doi.org/10.1016/j.tws.2020.107425.

Natarajan, S., Baiz, P.M., Bordas, S., Rabczuk, T. and Kerfriden, P. (2011a), "Natural frequencies of cracked functionally graded material plates by the extended finite element method", *Compos. Struct.*, **93**(11), 3082-3092. https://doi.org/10.1016/j.compstruct.2011.04.007.

Natarajan, S., Baiz, P.M., Ganapathi, M., Kerfriden, P. and Bordas, S. (2011b), "Linear free flexural vibration of cracked functionally graded plates in thermal environment", *Comput. Struct.*, **89**, 1535-1546. https://doi.org/10.1016/j.compstruc.2011.04.002.

Nguyen-Thoi, T., Rabczuk, T., Ho-Huu, V., Le-Anh, L., Dang-Trungm, H. and Vo-Duy, T. (2017), "An extended cell-based smoothed three-node Mindlin plate element (XCS-MIN3) for free vibration analysis of cracked FGM plates", *Int. J. Comput. Meth.*, **14**(2), 1750011. https://doi.org/10.1142/S0219876217500116.

Peng, L.X., Tao, Y.P., Liang, K., Li, L.Y., Qin, X., Zeng, Z.P. and Teng, X.D. (2017), "Simulation of a crack in stiffened plates via a meshless formulation and FSDT", *Int. J. Mech. Sci.*, **131**, 880-893. https://doi.org/10.1016/j.ijmecsci.2017.07.063.

Rahimabadi, A.A., Natarajan, S. and Bordas, S.P.A. (2013), "Vibration of functionally graded material plates with cutouts & cracks in thermal environment", *Key Eng. Mater.*, **560**, 157-180. https://doi.org/10.4028/www.scientific.net/KEM.560.157.

Raza, A., Talha, M. and Pathak, H. (2021), "Influence of material uncertainty on vibration characteristics of higher-order cracked functionally gradient plates using XFEM", *Int. J. Appl. Mech.*, **13**(5), 2150062. https://doi.org/10.1142/S1758825121500629.

Shahverdi, H. and Navardi, M.M. (2017), "Free vibration analysis of cracked thin plates using generalized differential quadrature element method", *Struct. Eng. Mech.*, **62**(3), 345-355. https://doi.org/10.12989/sem.2017.62.3.345.

Sinha, G.P. and Kumar, B. (2020), "Review on vibration analysis of functionally graded material structural components with cracks", *J. Vib. Eng. Technol.*, **9**(1), 23-49. https://doi.org/10.1007/s42417-020-00208-3.

Stahl, B. and Keer, L.M. (1972), "Vibration and stability of cracked rectangular plates", *Int. J. Solid. Struct.*, **8**(1), 69-91. https://doi.org/10.1016/0020-7683(72)90052-2.

Swaminathan, K., Naveenkumar, D.T., Zenkour, A.M. and Carrera, E. (2015), "Stress, vibration and buckling analyses of FGM plates-A state-of-the-art review", *Compos. Struct.*, **120**, 10-31.

Tran, L.V., Ly, H.A., Wahab, M.A. and Nguyen-Xuan, H. (2015), "Vibration analysis of cracked FGM plates using higher-order shear deformation theory and extended isogeometric approach", *Int. J. Mech. Sci.*, **96-97**, 65-78.

https://doi.org/10.1016/j.ijmecsci.2015.03.003.

Yang, G., Hu, D., Han, X. and Ma, G.W. (2017), "An extended edge-based smoothed discrete shear gap method for free vibration analysis of cracked Reissner-Mindlin plate", *Appl. Math. Model.*, **51**, 477-504. https://doi.org/10.1016/j.apm.2017.06.046.

Yang, H.S. and Dong, C.Y. (2019), "Adaptive extended isogeometric analysis based on PHT-splines for thin cracked plates and shells with Kirchhoff-Love theory", *Appl. Math. Model.*, **76**, 759-799. https://doi.org/10.1016/j.apm.2019.07.002.

Yang, H.S., Dong, C.Y., Qin, X.C. and Wu, Y.H. (2020), "Vibration and buckling analyses of FGM plates with multiple internal defects using XIGA-PHT and FCM under thermal and mechanical loads", *Appl. Math. Model.*, **78**, 433-481. https://doi.org/10.1016/j.apm.2019.10.011.

Yin, S., Yu, T., Bui, T.Q., Liu, P. and Hirose, S. (2016), "Buckling and vibration extended isogeometric analysis of imperfect graded Reissner-Mindlin plates with internal defects using NURBS and level sets", *Comput. Struct.*, **177**, 23-38. https://doi.org/10.1016/j.compstruc.2016.08.005.

Yuan, J. and Dickinson, S.M. (1992), "The flexural vibration of rectangular plate systems approached by using artificial springs in the Rayleigh-Ritz method", *J. Sound Vib.*, **159**(1), 39-55. https://doi.org/10.1016/0022-460X(92)90450-C.

Zhang, J.K., Yu, T.T and Bui, T.Q. (2021), "An adaptive XIGA with local refined NURBS for modeling cracked composite FGM Mindlin-Reissner plates", *Eng. Comput.*, **8**(4), 3639-3661. https://doi.org/10.1007/s00366-021-01334-6.

Zhang, N., Khan, T., Guo, H.M., Shi, S.S., Zhong, W. and Zhang, W.W. (2019), "Functionally graded materials: An overview of stability, buckling, and free vibration analysis", *Adv. Mater. Sci. Eng.*, **2019**, Article ID 1354150. https://doi.org/10.1155/2019/1354150.

CC